UNIVERSITY OF CALIFORNIA SAN DIEGO

Interactions between SMARCB1 and neural developmental state in cellular differentiation and carcinogenesis

A dissertation submitted in partial satisfaction of the
requirements for the degree Doctor of Philosophy

in

Biomedical Sciences

by

Alison Parisian

Committee in charge:

Professor Frank Furnari, Chair
Professor Rafael Bejar
Professor Alysson Muotri
Professor Lorraine Pillus
Professor Robert Wechsler-Reya
Professor Gene Yeo

2020

The Dissertation of Alison Parisian is approved, and it is acceptable in quality and form for publication on microfilm and electronically:

_____

_____

_____

_____

_____

_____

Chair

University of California San Diego

2020

DEDICATION

To my wonderful parents, who instilled in me a love of science at an early age and whose faith in me has always inspired me to reach further than I thought possible. And to Jimmy, who brightens my life and whose love and support makes even the most challenging times manageable.

TABLE OF CONTENTS

LIST OF ABBREVIATIONS

ARID1A AT-Rich Interaction Domain 1A

ATP Adenosine Triphosphate

ATRT Atypical Teratoid Rhabdoid Tumor

BAF BRG1- or BRM-Associated Factors

BMP Bone Morphogenetic Protein

BRG1 Brahma-related Gene 1

BRM Brahma

Cas9 CRISPR associated protein 9

ChIP-seq Chromatin ImmunoPrecipitation sequencing

Cre Cyclic Recombinase

CRISPR Clustered Regularly Interspaced Short Palindromic Repeats

CRISPRi Clustered Regularly Interspaced Short Palindromic Repeats interference

CTRL Control

dCas9 nuclease-dead Cas9

DCX Doublecortin

Dox Doxycycline

EZH2 Enhancer Of Zeste 2 Polycomb Repressive Complex 2 Subunit

FACS Fluorescence-Activated Cell Sorting

GFP Green Fluorescent Protein

H3K27Ac Histone H3 Lysine 27 Acetylation

HDR Homology Directed Repair

HES1 Hes Family BHLH Transcription Factor 1

HOX Homeobox

Indel Insertion or Deletion of nucleotides

iPSC induced Pluripotent Stem Cells

KD Knockdown

KRAB Krüppel associated box

LoxP Locus of X-over P1

mRNA messenger RNA

MRT Malignant Rhabdoid Tumors

MYC MYC Proto-Oncogene, BHLH Transcription Factor

NCAM Neural Cell Adhesion Molecule

NE Neuroepithelial

NFR Nucleosome Free Region

NHEJ Non-Homologous End-Joining

NOTCH Notch Receptor

NPC Neural Progenitor Cell

ORF Open Reading Frame

PAX6 Paired Box 6

PCA Principal Component Analysis

PCR Polymerase Chain Reaction

PRC2 Polycomb Repressive Complex 2

RFP Red Fluorescent Protein

RISC RNA-induced silencing complex

RNA-seq RNA sequencing

RT-PCR Real-Time PCR

scRNA-seq single-cell RNA sequencing

sgRNA single-guide RNA

SHH Sonic Hedgehog Signaling Molecule

shRNA short hairpin RNA

siRNA short interfering RNA

SMARCA2 SWI/SNF-Related Matrix-Associated Actin-Dependent Regulator Of Chromatin Subfamily A Member 2

SMARCA4 SWI/SNF-Related Matrix-Associated Actin-Dependent Regulator Of Chromatin Subfamily A Member 4

SMARCB1 SWI/SNF-Related Matrix-Associated Actin-Dependent Regulator Of Chromatin Subfamily B Member 1

SOX2 SRY-Box Transcription Factor 2

SWI/SNF SWItch/Sucrose Non-Fermentable

TGF-beta Transforming Growth Factor Beta

tSNE t-distributed Stochastic Neighbor Embedding

TSS Transcription Start Site

TYR Tyrosinase

UMI Unique Molecular Identifiers

UTR Untranslated Region

Wnt Wingless-related integration site

LIST OF FIGURES

LIST OF TABLES

ACKNOWLEDGEMENTS

I've been so lucky to be part of a wonderful community of friends, family and coworkers who have helped me get to where I am today.

Frank, thank you for being my mentor and for providing me with the resources and opportunities to learn new things and tackle new challenges. I have learned so much in your lab, and appreciate all that you've invested in me over the past five years. Thank you for all your support.

To my lab family, who have invested their time and energy into making me a better scientist and have made lab a welcoming and fun place to be, thank you for everything! In particular Pam, Amy, and Tomo: the three of you have made me into the research scientist I am today and I appreciate everything that you taught me.

To the members of my committee, thank you for taking the time to think about and provide input on this project. I appreciate the respect you've shown me and all of the help you've provided over the years.

To my friends, you have helped keep me happy and sane throughout this process. Thank you!

Jimmy, thank you for your patience with all the weekends spent in lab and for always supporting me when I'm stressed. You have helped me get through the hardest parts of graduate school and I'm so thankful to have you in my life.

Mom and Dad, you have always supported me in anything I wanted to do and taught me the value of hard work. I couldn't have done it without you!

Chapters 3 and 4, along with portions of Chapter 2, are a modified reprint of the material as it appears in Parisian AD, Koga T, Miki S, Johann PD, Kool M, Crawford JR, Furnari FB (2020). ”SMARCB1 loss interacts with neuronal differentiation state to block maturation and impact cell stability.” Genes & Development. The dissertation author was the primary author of this paper, conducted most of the included experiments and data analysis, and wrote the manuscript.

VITA

2010-2011	Summer Undergraduate Research Fellow, Barton Lab
	California Institute of Technology
2012	Summer Undergraduate Research Fellow, Bowie Lab
	University of California Berkeley
2013	Bachelor of Science in Biology
	California Institute of Technology
2015-2020	Graduate Research Fellow, Furnari Lab
	University of California San Diego
2020	Doctor of Philosophy in Biomedical Sciences
	University of California San Diego

PUBLICATIONS

Parisian AD, Koga T, Miki S, Johann PD, Kool M, Crawford JR, Furnari FB. 2020. SMARCB1 loss interacts with neuronal differentiation state to block maturation and impact cell stability. *Genes and development*.

Koga T, Chaim IA, Benitez JA, Markmiller S, Parisian AD, Hevner RF, Turner KM, Hessenauer FM, D'Antonio M, Nguyen N et al. 2020. Longitudinal assessment of tumor development using cancer avatars derived from genetically engineered pluripotent stem cells. *Nature Communications* 11: 550.

Orellana L, Thorne AH, Lema R, Gustavsson J, Parisian AD, Hospital A, Cordeiro TN, Bernadó P, Scott AM, Brun-Heath I et al. 2019. Oncogenic mutations at the EGFR ectodomain structurally converge to remove a steric hindrance on a kinase-coupled cryptic epitope. *Proceedings of the National Academy of Sciences* 116: 10009-10018.

Jameson NM, Ma J, Benitez J, Izurieta A, Han JY, Mendez R, Parisian A, Furnari F. 2019. Intron 1–Mediated Regulation of EGFR Expression in EGFR-Dependent Malignancies Is Mediated by AP-1 and BET Proteins. *Molecular Cancer Research*, 17: 2208-2220.

Zanca C, Villa GR, Benitez JA, Thorne AH, Koga T, D'Antonio M, Ikegami S, Ma J, Boyer AD, Banisadr A et al. 2017. Glioblastoma cellular cross-talk converges on NF-kappaB to attenuate EGFR inhibitor sensitivity. *Genes and development* 31: 1212-1227.

ABSTRACT OF THE DISSERTATION

Interactions between SMARCB1 and neural developmental state in cellular differentiation and carcinogenesis

by

Alison Parisian

Doctor of Philosophy in Biomedical Sciences

University of California San Diego, 2020

Professor Frank Furnari, Chair

Atypical teratoid rhabdoid tumors (ATRT) are challenging pediatric brain cancers which are predominantly associated with inactivation of the gene SMARCB1, a conserved subunit of the chromatin remodeling BAF complex, which has known contributions to developmental processes. To identify potential interactions between SMARCB1 loss and the process of neural development, we introduced an inducible SMARCB1 loss of function system into human induced pluripotent stem cells (iPSCs) which were subjected to either directed neuronal differentiation or differentiation into cerebral organoids. Using this system, we have identified substantial differences in the downstream effects of SMARCB1 loss depending on differentiation state

and identified an interaction between SMARCB1 loss and neural differentiation pressure which causes a resistance to terminal differentiation and a defect in maintenance of a normal cell state. Our results provide insight into how SMARCB1 loss might interact with neural development in the process of ATRT tumorigenesis.

Chapter 1

Introduction to SMARCB1 and Atypical Teratoid Rhabdoid Tumors

1.1 Atypical teratoid rhabdoid tumors

Atypical teratoid rhabdoid tumors (ATRTs) are challenging pediatric brain tumors which are predominantly associated with inactivation of the gene SMARCB1. ATRT accounts for 10-20% of pediatric brain cancer in children less than 3 years of age (1). With a median age of onset of 11 months and a lethality rate of 80-90% (2), these tumors are responsible for a huge loss of potential life. ATRTs are histologically heterogeneous tumors, and have demonstrated expression of several markers typical of pluripotent stem cells (3). The presence of cells from multiple germ layers within the same tumor, combined with stem cell marker expression and early age of onset suggest that ATRT may arise from pluripotent or multipotent stem cells. Few effective therapies are available for the treatment of ATRT and treatment is complicated by the negative cognitive effects of brain radiation in young children (4). Targeted therapeutics could provide a much-needed alternative to radiation, but none are yet approved for treatment of ATRT (although inhibitors against a few targets such as EZH2 (5) and Aurora Kinase A (6) have entered clinical trial). The identification and testing of additional therapies would be aided by a greater understanding of the mechanisms driving ATRT tumorigenesis and access to additional model systems with relevance to the human disease.

The genetic underpinnings of ATRT are simple, with virtually all tumors possessing a

deletion or mutation of the SMARCB1 locus in chromosome 22 (7, 8). SMARCB1 deletion has been shown to be both sufficient and necessary for ATRT tumorigenesis. Reintroduction of SMARCB1 to ATRT cell lines results in cell cycle arrest and reduced growth (9), while induced deletion of SMARCB1 in mice leads to developmentally restricted tumor formation in multiple models (10-12). In addition, the mutation rate in ATRT is very low (8), with no other consistent recurrent mutations identified. This low number of mutations is consistent with the early age of onset, but also implies that SMARCB1 loss must be able to initiate a wide range of transcriptional changes in order to induce tumorigenesis without the need for additional cooperative mutations.

Although SMARCB1 mutations are the sole known drivers for ATRT development, three tumor subtypes have been identified based on differences in transcriptional and epigenetic signatures (13, 14). These subtypes were identified independently in two separate studies and so two different naming schemes exist. However, the trends of mutation type, age of onset and unique classes of transcriptional and epigenetic drivers seem consistent across studies, indicating that a robust biological mechanism likely exists for the development of these three distinct types of ATRT. All three subtypes possess underlying SMARCB1 mutations, but the prevalence of mutation types has been shown to vary with subtype (13, 14). SHH/Group 1 tumors tend to be driven by smaller loss of function point mutations of SMARCB1, while MYC/Group 2B is frequently driven by focal alterations of the SMARCB1 locus and in TYR/Group 2A larger deletions of chromosome 22, containing SMARCB1, are more common. Subtype-specific differences in age of onset have also been identified, with the MYC/Group 2B subtype being more prevalent in older children (13, 14). Subtypes have been shown to have substantial differences in global DNA methylation levels (15), chromatin landscapes (13), and therapeutic sensitivities (13) in addition to distinct transcriptional drivers. Analysis of likely subtype-specific drivers based on RNA sequencing and enhancer profiling revealed increased expression of neurogenic genes including those associated with glutamate receptor signaling and axonal guidance along with genes associated with SHH and NOTCH signaling in the Group 1/SHH subtype (13, 14). Group 2A/TYR tumors display increased expression of the tyrosine metabolism pathway along with

genes associated with ciliogenesis and visual cortex or hindbrain development (13, 14), while Group 2B/MYC tumors are characterized by overexpression of the MYC oncogene and HOX cluster genes (13, 14). A more recent paper conducted single-cell RNA sequencing on ATRT and compared to transcriptional profiles of pediatric and embryonic cell types (16). This data showed that the Group1/SHH subtype bears the greatest similarity of neuroectoderm tissue types of the early embryo, while the other two subtypes more closely resemble non-neural tissue types. This is also consistent with a comparison between ATRT subtypes and SMARCB1-deficient malignant rhabdoid tumors (MRTs) from other tissue types, which found high transcriptional similarity between MRTs and the MYC/Group2B subtype (15). Thus, it seems likely that cell type of origin might play a role in driving differences between subtypes.

1.2 SMARCB1 and the BAF complex

The SMARCB1 gene encodes a subunit of the BAF (also known as SWI/SNF) chromatin remodeling complex. Thus, its effects on gene expression and tumorigenesis result from changes in regulation of chromatin architecture. Gene expression relies not only on the expression of necessary transcription factors, but also on the ability of DNA-binding proteins to access the appropriate transcription start site and regulatory regions. This access is regulated by the position of nucleosomes, the primary packaging unit of chromatin. A nucleosome consists of 147 base pairs of DNA wrapped around a histone octamer and blocks access to one face of the associated DNA, limiting recognition and binding by other proteins (17). Nucleosome positions are determined partly by an intrinsic sequence preference of histone octamers for particular regions of DNA (18), but chromatin remodeling complexes also play important regulatory roles by controlling the density and position of nucleosomes as well as the positions of activating histone variants (17).

Nucleosomes are positioned around genes in a consistent manner, with a low-density nucleosome free region (NFR) upstream of and through the transcription start site (TSS). The

NFR is flanked by two consistently positioned nucleosomes; the -1 nucleosome upstream of the NFR must be evicted for transcription machinery to assemble and for transcription to occur, while the position of the +1 nucleosome immediately downstream is tightly coupled to the position of the TSS and may be involved in positioning of transcription factors (19). Positioning and density of nucleosomes can have powerful effects on the ability of particular genes to be transcribed. It has also been suggested that nucleosomes have important roles in suppressing inappropriate antisense transcription (20). When taken together the 20 BAF subunit genes have been shown to be mutated in 19% of all tumor types (21). This speaks to the important genome-wide regulatory role of this complex.

The BAF complex uses ATP hydrolysis to restructure chromatin through breaking DNA-histone interactions, sliding histones along DNA, ejecting histones or histone dimers, and enhancing transcription factor binding (17). These alterations of nucleosome positioning and occupancy (17) can lead to downstream changes in chromatin accessibility (22, 23) and enhancer activity (24, 25). BAF complex subunit composition can be quite diverse. The complex contains four invariable core subunits, including one of two mutually exclusive catalytic subunits (SMARCA4, aka BRG1, and SMARCA2, aka BRM). While SMARCB1 is one of these core subunits, it is not responsible for the catalytic histone remodeling activity. SMARCB1 acts as a scaffold protein and is important for maintaining the structural stability of the complex (26). While loss of SMARCB1 does not prevent complex formation (27), its loss does lead to reduced incorporation and increased degradation of multiple subunits (24, 28). Structural studies on the interactions between the yeast SWI/SNF complex and nucleosomes suggest that SMARCB1 may also be directly involved in maintaining histone contacts during the remodeling process (26). Tumorigenesis resulting from SMARCB1 deletion has been shown to depend on the presence of the SMARCA4 catalytic subunit (29). This suggests that loss of SMARCB1 may promote tumor formation through an altered or gain of function of the BAF complex rather than a reduction in complex activity.

In addition to its likely role as a tumor suppressor, the BAF complex has important roles

in development and cellular differentiation. Nucleosomal occupancy changes are an important aspect of the epigenetic alterations that take place during cellular differentiation (30), and the BAF complex in general along with SMARCB1 in particular are important regulators of normal nucleosomal occupancy patterns (23, 31). Multiple forms of the BAF complex exist (32, 33), with subunit composition changing as pluripotent cells differentiate (34, 35), and a distinct version of the complex with defined subunit composition has been identified in stem cells (32). The BAF complex has been implicated in differentiation down adipocyte, hematopoietic, hepatocyte, neural and osteoblast lineages (36), and homozygous deletion of SMARCA4 or SMARCB1 are embryonic lethal in mouse models (10). In addition, members of the complex have been identified as reprogramming factors to generate pluripotent cells from somatic cells (37). The sufficiency of SMARCB1 deletion to drive pediatric tumor growth but the paucity of SMARCB1 mutations in adult cancers, along with the demonstrated role of the BAF complex in development and differentiation leads us to the hypothesis that the ability of SMARCB1 deletion to cause tumorigenesis may be dependent on the epigenetic environment of a particular cell type or stage of differentiation.

1.3 Mechanisms of ATRT tumorigenesis

While the precise mechanisms of tumorigenesis resulting from SMARCB1 loss are not entirely clear, it is known that a variety of epigenetic changes take place in SMARCB1-deficient tumors. SMARCB1 loss has been shown to contribute to changes in chromatin structure and defects in the maintenance of nucleosome positioning (23). In addition, ATRTs display changes in DNA methylation profiles which can vary between subtypes (13, 14) and can range from a global hypermethylation phenotype to depletion of methylation levels. Substantial changes have also been detected in genome-wide enhancer profiles in the absence of SMARCB1, along with changes in the ability of the BAF complex to bind at enhancer regions (24). Enhancer profiles of ATRTs can be subtype-specific, with drivers of each subtype marked by active enhancers not

present in tumors of other subtypes (13, 14). These studies indicate that SMARCB1 loss can lead to dramatic and widespread changes in the epigenome and that these changes vary with the subtype of the tumor.

It has been shown that SMARCB1 loss can lead to increased activity of the polycomb repressive complex 2 (PRC2) (22, 38). The PRC2 complex catalyzes the methylation of histone H3 at lysine 27, an important epigenetic mark which promotes chromatin compaction and has a repressive effect on gene expression (39). The BAF complex and PRC2 have been shown to compete for binding sites, and to have antagonistic effects on both chromatin structure and gene expression (22). Increased PRC2 activity in SMARCB1-deficient cells has been suggested to play a prominent role in the transcriptional and epigenetic changes resulting from SMARCB1 loss (Figure 1.1) and contributes to tumor growth (38). Increased PRC2 binding due to loss of SMARCB1 (38), skewed SMARCB1-deficient BAF complex binding at superenhancers (24), and resulting downstream epigenetic and transcriptional changes have been suggested mechanisms of tumorigenesis in ATRT, but many questions still remain unanswered. It seems likely that subtype-specific differences, and possibly the ability of SMARCB1 loss to initiate tumorigenesis, could arise from initial epigenetic differences in cells of various cell types and stages of differentiation. My goal in this thesis project is to elucidate the importance of cell type for ATRT tumorigenesis by developing a SMARCB1-deficient pluripotent cell line which can be subjected to differentiation into cell types of interest.

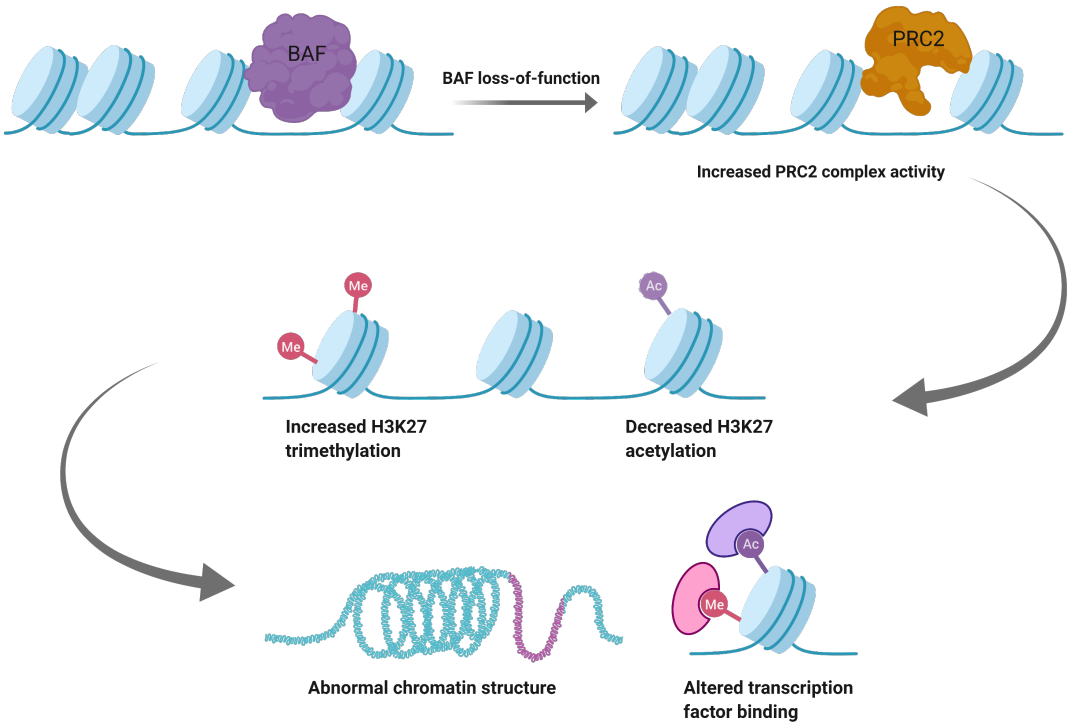

Figure 1.1. Epigenetic changes resulting from BAF complex loss of function. Schematic showing how BAF complex loss of function can lead to gene expression changes through a variety of genome-wide epigenetic alterations caused by reduced BAF complex binding and a corresponding increase in PRC2 complex binding.

Chapter 2

Engineering a SMARCB1-deficient model of Atypical Teratoid Rhabdoid Tumors (ATRT) using induced pluripotent stem cells

2.1 Introduction

A cellular model of ATRT that accurately recapitulates the low-mutation genetic background of these tumors along with the likelihood of multipotent cells of origin has not yet been generated and could be a critical step towards the identification of effective therapeutics for this fatal disease. Several SMARCB1-deficient mouse models have been generated (10-12, 40), but these have limitations for application to the human disease. Early SMARCB1-deficient mouse models displayed low penetrance of tumor formation (40) or lead to the development of tumors in cell types and tissues inconsistent with the human disease (10). More recent models utilizing inducible knockouts in particular tissues or stages of development (11, 12) have improved upon these issues, but it is difficult to directly manipulate and monitor the interactions between differentiation state and SMARCB1 loss using an in vivo system, and a cell-based model with isogenic control is preferable for drug screening applications. In addition, a human model may outperform a mouse model in some situations due to the greater genetic and epigenetic resemblance to the human disease.

Engineering of induced pluripotent stem cells (iPSCs) with known tumorigenic alterations has been shown to be an effective technique for modeling of glioblastoma (41), and the paucity of mutations in ATRT make it a particularly good candidate for this type of modeling. An iPSC-based system would also enable manipulation of cellular differentiation state in order to monitor cell type-specific differences in the phenotypic and transcriptional impacts of SMARCB1 loss and identify cell types or stages of differentiation with differential sensitivity to the loss of SMARCB1. Initially it was decided to generate this SMARCB1-deficient iPSC line through genetic mutation of the SMARCB1 locus using CRISPR-Cas9 genome editing technology.

2.2 CRISPR-Cas9-mediated deletion of the SMARCB1 locus

2.2.1 Design of CRISPR-Cas9 knockout strategy

CRISPR-Cas9 genome editing allows precise targeted cleavage at a particular region of the genome through use of a guide RNA (sgRNA) with the appropriate sequence, which interacts with the Cas9 nuclease protein to direct its double-strand cleavage (42). Low rates of off-target cleavage have been observed in human pluripotent stem cells (43). Genetic deletion of the full chromosomal region containing SMARCB1 or a portion of the gene region is frequently observed in ATRT (13, 14), and the precision of Cas9-targeted cleavage combined with the ability to use multiple guide RNAs simultaneously (44) allows for accurate recapitulation of these genetic events.

Pairs of CRISPR-Cas9 sgRNAs were designed for inactivation of SMARCB1 through full gene excision as well as through removal of SMARCB1 exon 2, leading to loss-of-function through frameshift mutation and premature stop codon incorporation (Supplementary Table 2.1). Both of these types of genomic alterations have been observed in ATRT and are prevalent in different subtypes (13, 14). Generating both would allow a determination of whether deletion of SMARCB1 intronic regions might play a role in ATRT tumorigenesis or affect cellular

transcriptional or epigenetic profiles. In both cases, deletion would occur with simultaneous cleavage at both sgRNA target sites and subsequent repair by the non-homologous end-joining (NHEJ) mechanism, in which double-strand breaks are repaired by ligation without use of a repair template. This results in removal of the intervening segment of DNA in some cells, which can be screened for by PCR amplification of the edit region to identify cells with the desired edit. For full-gene deletion, sgRNA sequences were designed to target Cas9-mediated cleavage in the first and last exons of SMARCB1. For exon 2 deletion, sgRNA sequences were targeted in introns 1 and 2 flanking the exon (Figure 2.1, Supplementary Table 2.1).

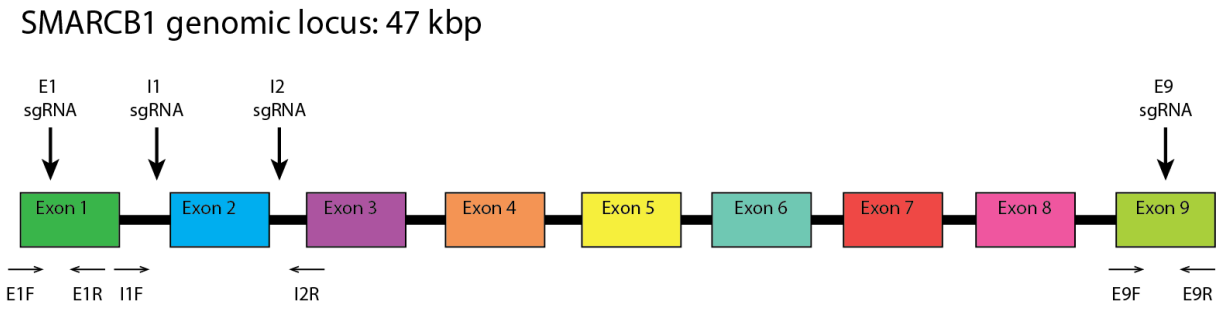

Figure 2.1. SMARCB1 deletion strategy. Design of CRISPR-Cas9 sgRNAs (top) and PCR primers (bottom) for either full gene deletion of SMARCB1 (E1/E9 sgRNAs and primers) or induction of frameshift through deletion of exon 2 (I1/I2 sgRNAs and primers).

2.2.2 Generation and testing of CRISPR-Cas9 knockout constructs

sgRNA sequences were cloned into a Cas9-encoding construct (PX458) which also encodes a GFP fluorescent marker. Thus the Cas9 protein, sgRNA targeting construct and GFP marker can all be simultaneously introduced into the target cells. Cas9 and sgRNA constructs were validated using the 293T cancer cell line before applying to the more difficult to engineer iPSCs. Cells were transfected with the PX458 plasmid to target Cas9-mediated cleavage and transfected cells sorted for GFP expression. Sorted cells were screened for presence of the desired deletion by PCR amplification of the desired edit regions with primer sites shown in Figure 2.1. PCR product using exon 1 and exon 9 primers can only be obtained in the case of

successful full-gene deletion, as otherwise the distance between primer sites, which span the entire SMARCB1 locus (approximately 47.5 kbp), is too large for product generation. In cells with successful full-gene deletion, a PCR product of approximately 300 bp can be generated from even a small percentage of cells with successful deletion. PCR primers within introns 1 and 2 will form product in unedited cells (approximately 650 bp), but a lower molecular weight product (approximately 250 bp) is obtained with successful deletion of exon 2. PCR screening of transfected and GFP-sorted 293Ts was conducted using two sets of sgRNAs per target site, revealing successful generation of both full-gene and exon 2 deletion product in the bulk cell population with all sgRNA combinations (Figure 2.2A). SMARCB1 transcript levels of the edited population were quantified by real-time PCR (Figure 2.2B) to determine efficiency of knockdown in six combinations of sgRNAs. Efficiency of knockout was high enough that the top-performing sets of sgRNAs showed significant reductions in SMARCB1 transcript even in this bulk population (22.6% of unedited 293Ts for full-gene deletion and 43.4% for exon 2 deletion). This suggests both that these sgRNA pairs are highly effective at generating the desired deletion products and that these genetic deletions lead to a loss of SMARCB1 expression. Combinations of sgRNAs with the greatest reduction in transcript levels for each deletion type were chosen for application in iPSCs.

2.2.3 Application of CRISPR-Cas9 knockout constructs in iPSCs

For SMARCB1 deletion in iPSCs, the CV-iPS-B cell line (45) was electroporated with the top-performing CRISPR-Cas9 constructs identified using 293Ts. Cells were sorted for GFP, plated in a low concentration on matrigel-coated plates and allowed to form clonally-derived colonies while the bulk population was analyzed for presence of the desired deletion products. Using the same procedure applied to 293Ts, PCR of GFP-sorted iPSCs revealed successful formation of both full-gene and exon 2 deletion products (Figure 2.2C). To identify clones with homozygous SMARCB1 deletion for further studies, colonies were screened for presence of the desired mutations by PCR using the same primers applied to the bulk population along with

the addition of primers within the full-gene deletion region for detection of unedited genetic material. Forty-eight clones were screened for each sgRNA pair, and while eight clones were identified with full-gene deletion product and seven with exon 2 deletion product, all clones

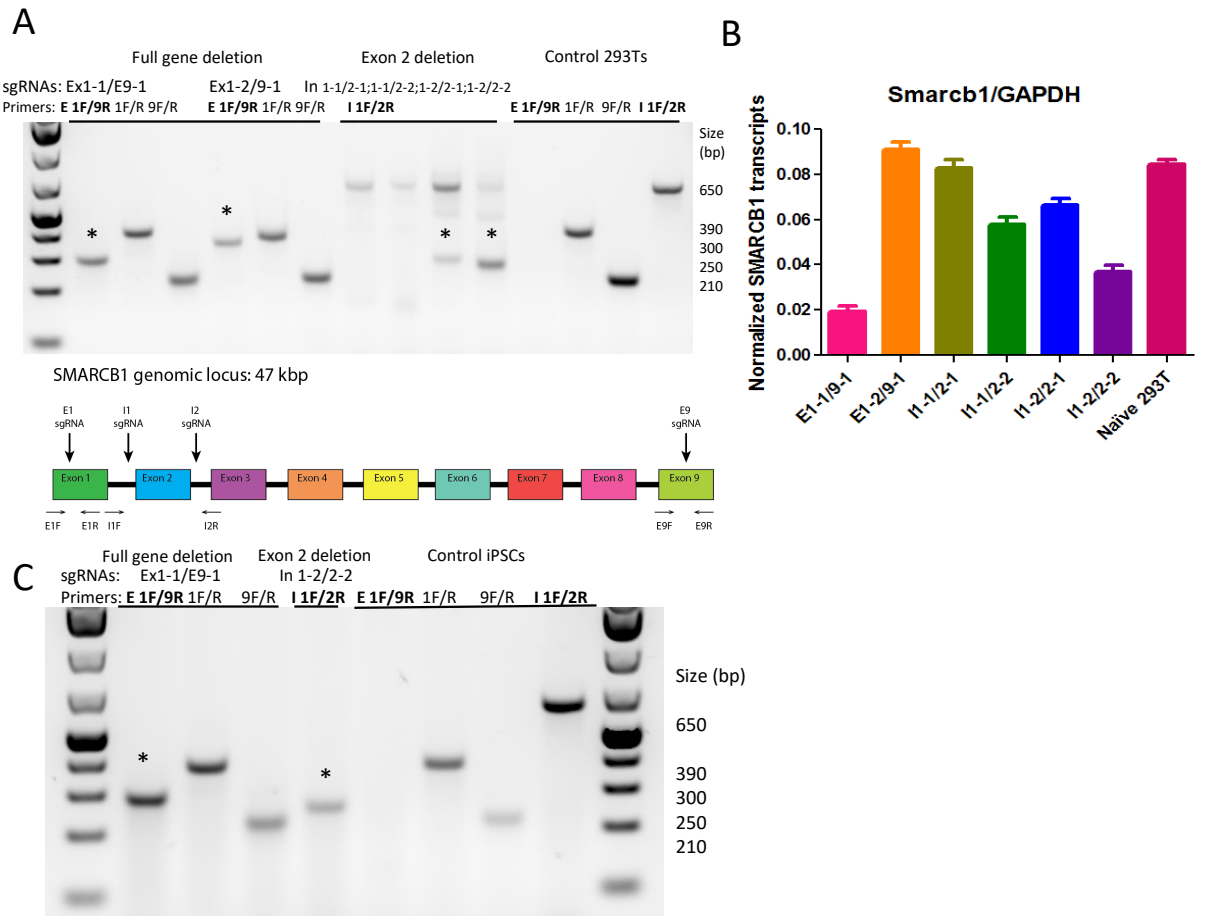

Figure 2.2. Testing of SMARCB1 knockout constructs in 293T cells and iPSCs. A) Genomic PCR analysis of GFP-sorted CRISPR-edited 293Ts with primers and sgRNAs shown below. Two sgRNAs were tested for each target site, with the exception of exon 9 for full gene deletion. Asterisks mark products which represent successful CRISPR editing of the desired region. B) Real-time PCR quantification of SMARCB1 transcript levels in GFP-sorted 293Ts after transfection of pairs of CRISPR-Cas9 editing constructs. Unedited control 293Ts are shown on right. Based on this data the sgRNA pair Ex1-1 and Ex9-1 was chosen for full gene deletion application to iPSCs and the pair In1-2 and In2-2 for exon 2 deletion. C) Genomic PCR analysis of GFP-sorted CRISPR-edited CV-B iPSCs with same primer sets used in 293Ts. Asterisks mark products which represent successful CRISPR editing of the desired region. Control unedited iPSCs are shown on right for comparison.

were ultimately found to be heterozygous, although the majority contained small insertions or deletions (indels) near the sgRNA target sites on the unedited allele, indicating successful CRISPR-Cas9-mediated cleavage but unsuccessful removal of the intervening region. These indels were not predicted to disrupt protein function. It was initially thought that this might be due to lower efficiency of transfection and manipulation in iPSCs compared to 293Ts, so a second round of editing was planned using the heterozygous clones. Alternate sgRNA pairs were chosen for each deletion type to avoid indels generated by the initial set of sgRNAs on the intact SMARCB1 allele and were tested in 293Ts for efficacy before electroporation into heterozygous clones. In spite of high editing efficacy of sgRNA pairs in initial tests, of 48 clones screened for each deletion type, all remained heterozygous for SMARCB1 deletion after the second round of editing. This substantially lower editing efficiency compared to the first round of SMARCB1 deletion suggested the likelihood of selective pressures against homozygous SMARCB1 deletion in iPSCs. The much higher rate of editing efficiency in 293Ts compared to iPSCs suggest that cell type-specific effects of SMARCB1 loss might be playing a role. Based on this, it was determined that an inducible form of SMARCB1 repression was needed to investigate possible lethality or growth defects at the iPS state as well as the possibility of cell type-specific differences in phenotype.

2.3 Application of CRISPR-Cas9 for engineering an inducible SMARCB1 knockout

In order to obtain the type of SMARCB1 focal deletions typically observed in ATRT in an inducible manner, a system was designed to incorporate LoxP sites flanking SMARCB1 exon 2 which, in conjunction with application of the Cre recombinase, would result in the removal of exon 2 and generation of a frame shift mutation to induce loss of function (Figure 2.3A). CRISPR-Cas9 constructs would be used to generate double-strand breaks in the vicinity of SMARCB1 exon 2, as described previously, but this time in combination with a donor plasmid

to induce incorporation of the desired edit near the sgRNA target site. Presence of a donor plasmid with homology to the region of the double-strand break initiates the homology directed repair (HDR) cellular repair process, using the donor plasmid as a template for repair of the double-strand break and incorporating the desired edit into the genomic DNA. Generation of a successful edit by HDR is generally less efficient than inducing loss of function deletions using the NHEJ process. To aid in the isolation of successfully edited cells, the donor plasmid was designed to incorporate a puromycin selection cassette downstream of the second LoxP site, within SMARCB1 intron 1 (Figure 2.3A). This donor plasmid was engineered using a combination of PCR amplification and restriction enzyme cloning. Unfortunately, when applied to SMARCB1 heterozygous iPSCs generated in Figure 2.2, few colonies were obtained after puromycin selection and those generated were negative for the desired edits (Figure 2.3B), suggesting possible non-specific integration of the donor plasmid or puromycin selection cassette. Again, this implies a likely biological selection against homology directed repair at the target site. While the intention of the edit design was to avoid interruptions to the SMARCB1 coding sequence prior to Cre introduction, it is possible that the incorporation of the LoxP sites or selection cassette resulted in disruption to SMARCB1 expression and was selected against. Given the resistance of iPSCs to genetic editing of the SMARCB1 locus, it was decided that an inducible SMARCB1 knockdown system would prove easier to engineer while providing the desired flexibility in timing of SMARCB1 loss.

Figure 2.3. Inducible SMARCB1 deletion strategy. A) Editing schematic for inducible Cre-LoxP-mediated SMARCB1 knockout. CRISPR-Cas9 constructs were designed to incorporate LoxP sites flanking exon 2 and a puromycin selection cassette so that Cre application would result in exon 2 removal. B) Agarose gel of PCR product generated from puromycin-selected iPSC clones after electroporation with CRISPR-Cas9 editing constructs and donor plasmid to incorporate LoxP sites and puromycin selection cassette. PCR was conducted using either an external primer set with primer sites outside of the donor plasmid homology region (top gel) or an internal primer set with primer sites flanking exon 2 (bottom gel). None of these clones display positive integration product in spite of their puromycin resistance, suggesting possible non-specific integration.

A

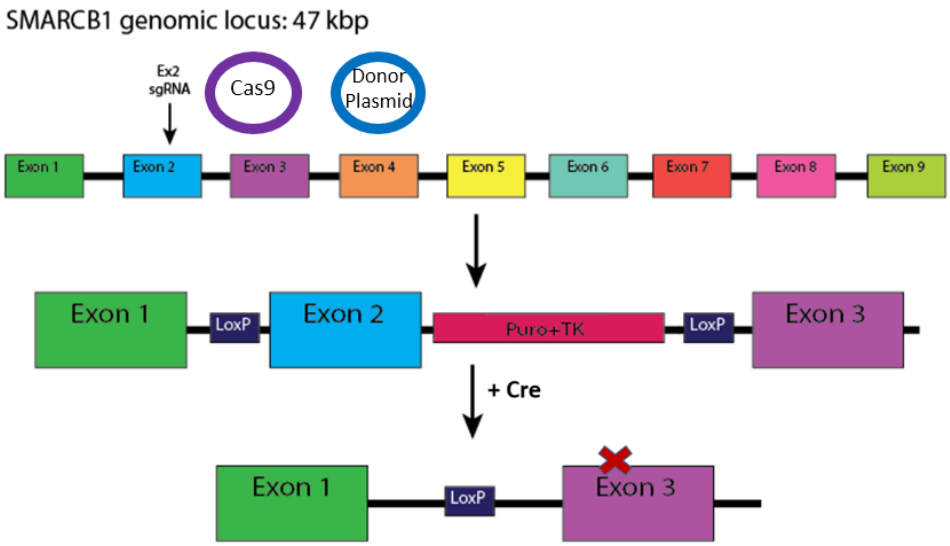

B

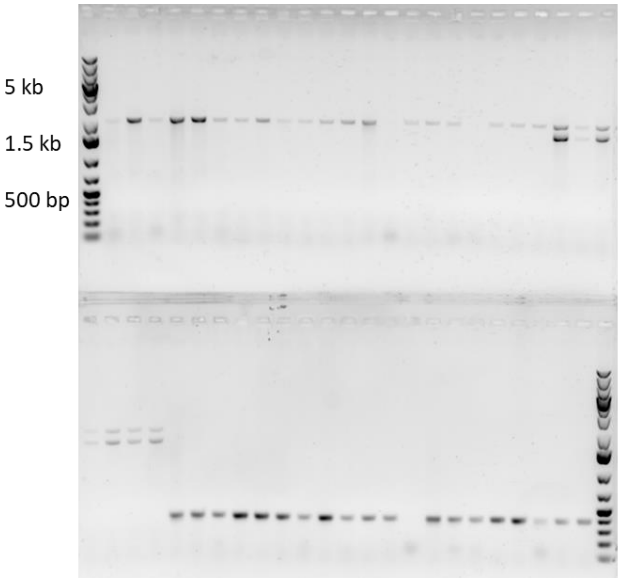

With integration: 5 kb product
No integration: 2.5 kb product

With integration: 3 kb product
No integration: 400 bp product

5 kb

1.5 kb

500 bp

2.4 Generation of an inducible SMARCB1 knockdown cell line using doxycycline-inducible shRNA constructs

Two alternate methods of inducible SMARCB1 knockdown were applied in distinct iPSC lines: short hairpin RNA (shRNA) and CRISPR interference (CRISPRi). shRNA is a form of RNA interference technology in which DNA sequences introduced through a plasmid or lentiviral particle are transcribed by normal cellular processes, forming the shRNA. This shRNA is then cleaved by the endogenous Dicer enzyme to generate smaller short interfering RNA (siRNA) sequences. These fragments associate with the RNA-induced silencing complex (RISC), allowing it to recognize and cleave its target mRNA, leading to further degradation of the transcript. This mechanism varies significantly from CRISPRi, which contains a nuclease-dead version of the Cas9 protein (dCas9) discussed earlier, tethered to a repressive KRAB domain. Just as in CRISPR editing, an sgRNA sequence is used to target Cas9 to a particular site in the genome. However, in the CRISPRi system the sgRNA is designed to target near the transcriptional start site (TSS) of the gene of interest in order to prevent binding and transcription initiation by RNA polymerase. Especially in conjunction with a tethered KRAB domain, this can effectively repress the expression of the gene of interest. In summary, while shRNA knockdown works by targeting transcripts for degradation, CRISPRi reduces the number of transcripts formed by blocking the transcription start site. This leads to several differences in the application and efficacy of these techniques. Because CRISPRi does not actively reduce the number of target gene transcripts in a cell, its ability to induce knockdown is slower than shRNA. It relies on normal cellular mechanisms to degrade target gene transcript and protein before an effect will be observed, while shRNA begins to actively degrade transcripts present in a cell as soon as the shRNA is expressed. Thus, shRNA can initiate effective knockdown within 24 hours, while CRISPRi may take several days to achieve an observable effect.

For shRNA knockdown of SMARCB1, three doxycycline-inducible shRNA constructs (Supplementary Table 2.3) were purchased encoding sequences predicted to target various

sites in SMARCB1 coding regions along with a puromycin selection cassette and doxycycline-inducible turboRFP marker (Figure 2.4A). These constructs were initially transfected into 293Ts for testing before being packaged into lentiviral vectors and transduced into iPSCs. Two of the three shRNA sequences were able to effectively reduce SMARCB1 transcript in 293Ts, although only one of these ultimately showed an effective reduction in protein levels (Figure 2.4B). Both of these shRNAs (designated sh658 and sh905) were chosen for transduction into iPSCs. shRNA constructs were transduced into the iPS12 iPSC line and puromycin selection applied to remove non-expressing cells. The resulting populations showed effective reduction in SMARCB1 transcript after 24 hours of doxycxyline treatment (Figure 2.4A), although sh905 reduced transcript levels further than sh658.

To generate inducible knockdown of SMARCB1 using CRISPRi, the engineered CRISPRi Gen1C cell line was obtained from the Conklin lab at UCSF (46). This cell line was engineered to express dCas9-KRAB along with the mCherry fluorescent marker from a doxycycline-inducible promoter (Figure 2.4C). Custom CRISPR sgRNAs were designed as described previously, but were focused around the SMARCB1 transcription start site (TSS) or downstream untranslated region (UTR). Six possible sgRNAs were designed (Supplementary Table 2.3), four of which were within one hundred base pairs of the SMARCB1 TSS and two of which were within the 5' UTR. These sgRNAs were incorporated into a construct which also encoded a blasticidin resistance cassette and mKate2 fluorescent marker. sgRNA constructs were electroporated into CRISPRi Gen1C cells, selected for successful sgRNA expression using blasticidin, and induced for 7 days with doxycycline prior to analysis of SMARCB1 transcript levels. Analysis of knockdown by RT-PCR in bulk population (data not shown) showed the strongest SMARCB1 knockdown with two sgRNAs (UTR1 and TSS1), which were chosen for further pursuit. However, knockdown was less efficient than was observed with shRNA, with total knockdown levels of only about 50%.

To increase knockdown levels as much as possible, 20-24 clonal populations were generated from each of the top two shRNA constructs and CRISPRi sgRNAs and analyzed

for SMARCB1 transcript levels (Figure 2.4A,C). CRISPRi clones showed higher variability in SMARCB1 levels than shRNA clones (Figure 2.4A,C). For each construct, the five clones with most effective SMARCB1 knockdown were chosen and pooled to generate a new population with more efficient knockdown of SMARCB1. Resulting populations of shRNA construct sh905 and CRISPRi construct UTR1 resulted in efficient loss of both SMARCB1 transcript and protein (Figure 2.4B, D). However, even after pooling the top-performing clones, shRNA construct sh658 and CRISPRi sgRNA TSS1 did not generate effective reduction in SMARCB1 protein levels (Figure 2.4B,D). sh905 and UTR1 were chosen for use in further experiments, and will hereafter be referred to as shSMARCB1 and CRISPRi SMARCB1, respectively.

Figure 2.4. Engineering of inducible SMARCB1 knockdown cell lines. A) Above, schematic of inducible shRNA construct used. Below, real-time PCR showing transcript levels after doxycycline induction of isolated clones from populations transduced with two separate shRNA constructs, sh905 and sh658. The five clones with lowest SMARCB1 expression levels were combined to form the cell line used in future experiments. B) Western blot of SMARCB1 protein levels in control and SMARCB1 shRNA lines after 3 days of doxycycline induction, in comparison to SMARCB1-deficient BT16 and G401 rhabdoid cell lines. sh658 only demonstrates a partial knockdown of SMARCB1 and so was not used in future experiments. C) Above, schematic of inducible CRISPRi system used. Below, real-time PCR showing transcript levels after doxycycline induction of isolated clones from populations transduced with two separate sgRNA constructs, UTR1 and TSS1. The five clones with lowest SMARCB1 expression levels were combined to form the cell line used in future experiments. B) Western blot of SMARCB1 protein levels in control and SMARCB1 targeting CRISPRi cell lines with and without 7 days of doxycycline induction, in comparison to SMARCB1-deficient BT12 and BT16 ATRT cell lines. sgRNA TSS1 only demonstrates a partial knockdown of SMARCB1 and so was not used in future experiments.

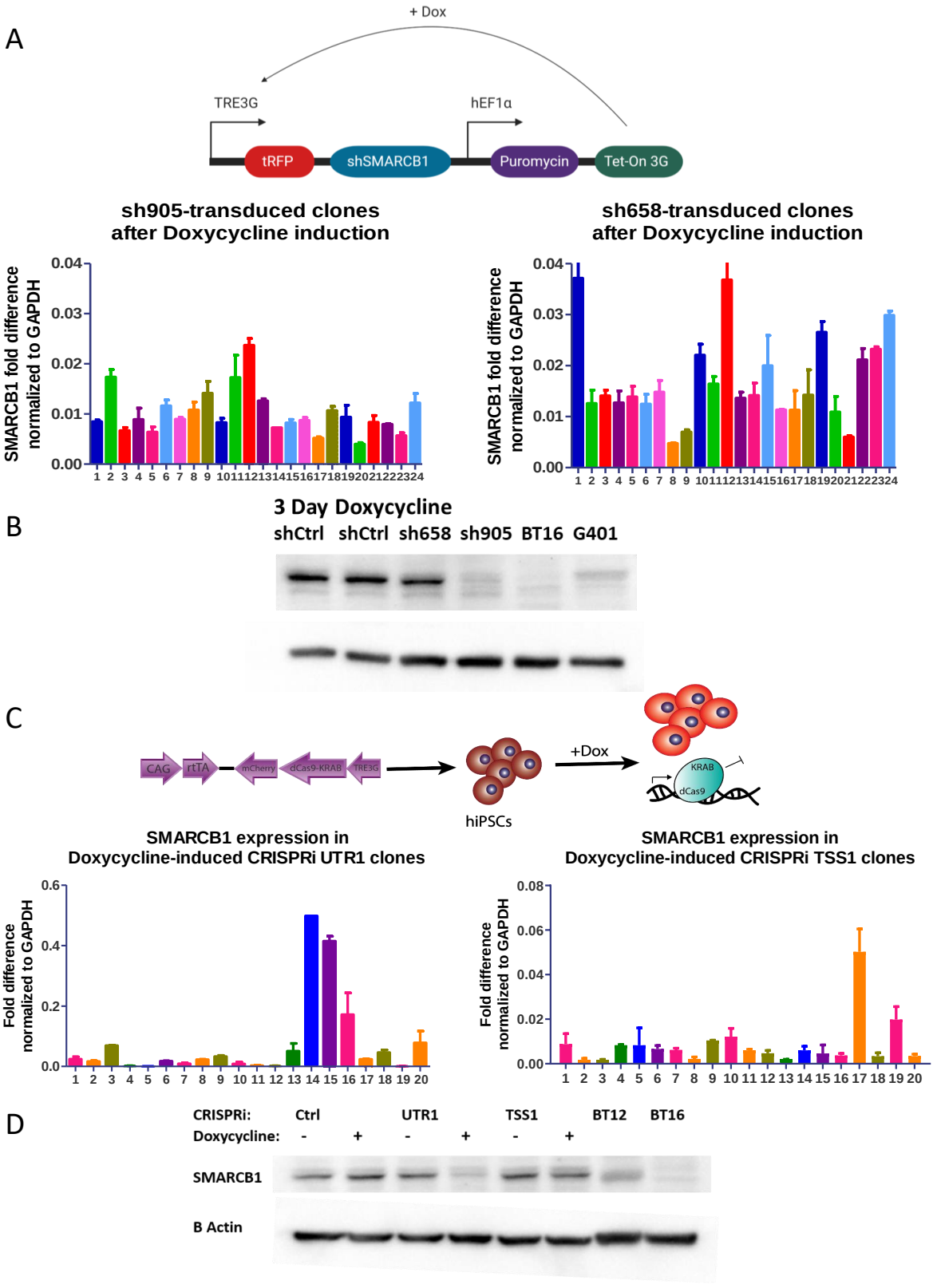
A
+ Dox
TRE3G
hEF1α
tRFP
shSMARCB1
Puromycin
Tet-On 3G
sh905-transduced clones
after Doxycycline induction
sh658-transduced clones
after Doxycycline induction
SMARCB1 fold difference
normalized to GAPDH
B
3 Day Doxycycline
shCtrl shCtrl sh658 sh905 BT16 G401
C
CAG
rtTA
mCherry
dCas9-KRAB
TRE3G
hiPSCs
+Dox
KRAB
dCas9
SMARCB1 expression in
Doxycycline-induced CRISPRi UTR1 clones
SMARCB1 expression in
Doxycycline-induced CRISPRi TSS1 clones
Fold difference
normalized to GAPDH
D
CRISPRi: Ctrl UTR1 TSS1 BT12 BT16
Doxycycline: - + - + - +
SMARCB1
B Actin

2.5 Perspectives and conclusions

In summary, the development of a SMARCB1-deficient iPSC line was pursued in order to effectively model the interactions between SMARCB1 loss and neural development and determine how these interactions might relate to the tumorigenesis of atypical teratoid rhabdoid tumors (ATRT). Initially CRISPR-Cas9 engineering was attempted to generate genetic knockout of SMARCB1 at the pluripotent state prior to differentiation down a neural lineage. However, this technique proved not to be viable in the cell type of interest, as homozygous clones were not able to be generated. It was concluded that SMARCB1 loss in pluripotent cells likely contributed to cell death or cellular growth defects which prevented the generation of viable SMARCB1-deficient clones.

To investigate this possibility and to effectively initiate SMARCB1 loss at various stages of differentiation, SMARCB1 knockdown was chosen as a viable and more flexible alternative to genetic knockout. Two forms of knockdown were pursued simultaneously: an shRNA knockdown method designed to degrade SMARCB1 transcript and a CRISPRi system for blocking the initiation of SMARCB1 transcription. A single construct from each method was identified which was capable of highly effective SMARCB1 knockdown at the iPS state and was chosen for additional experiments.

While lethality of SMARCB1 loss in pluripotent cells has not been demonstrated directly prior to this study, this hypothesis is consistent with published data from SMARCB1-deficient mouse models in which SMARCB1 loss was found to be embryonic lethal if homozygous loss of function occurred prior to embryonic stage E5 (11). Heterozygous mice, however, were viable with an increased tendency towards post-natal tumor formation (40). This is consistent with our ability to generate heterozygous SMARCB1 knockout clones but inability to retrieve homozygous SMARCB1 knockouts using pluripotent cells. While it may have been possible to induce CRISPR-Cas9 deletion of SMARCB1 at a later differentiation state, such as in neural progenitor cells, this would not give us the flexibility to investigate differences in effects

of SMARCB1 loss with differentiation stage. In addition, more differentiated cells are less amenable to manipulation and isolation of individual clones than pluripotent cells. The inducible SMARCB1 knockdown cells generated in these experiments can be applied to study the role of SMARCB1 in differentiation processes and investigate the role of cellular differentiation state in ATRT tumorigenesis. An isogenic model of ATRT using human cells can be adapted for applications such as investigating SMARCB1-induced changes in transcriptome and epigenetic state, tumor engraftment studies using mouse xenografts, and in vitro or in vivo drug screening.

2.6 Methods

2.6.1 CRISPR-Cas9 editing and screening

For CRISPR-Cas9 editing, pSpCas9(BB)-2A-GFP or PX458 plasmid which expresses Cas9-T2A-GFP, was purchased from Addgene (Plasmid 48138). sgRNA sequences were designed using the CRISPR-Cas9 design website https://chopchop.cbu.uib.no/ (47) (Supplementary table 2.1). Two suggested sgRNAs with best scores and target sites within 250bp of the region of interest were chosen for each cut site. Complementary oligos were generated for each sgRNA, annealed and cloned into the PX458 plasmid using the BbsI restriction enzyme. For homology directed repair editing, a donor plasmid was generated through restriction enzyme cloning to incorporate the desired edit sequence (ordered as customized oligos) as well as 250 bp homology regions on either side of the desired edit (amplified by PCR of genomic DNA). For incorporation of PX458 constructs (and donor plasmid if needed) into cells, 293Ts were transfected using Lipofectamine 2000 transfection reagent and CV-iPS-B cells were electroporated using the B-016 program of Lonza Nucleofector 2b and Lonza Human Stem Cell Nucleofector Kit 1 reagents. GFP-positive cells were sorted using an SH800 cell sorter. For initial analysis of sgRNA efficacy, DNA was extracted from the sorted population using a Qiagen miniprep kit and target regions amplified by PCR (Supplementary table 2.2). For derivation and screening of iPSC colonies, 1-2 $\times$ 10^4 cells were plated in a Matrigel-coated 10 cm tissue culture dish and allowed

to form visible colonies. After initial editing in iPSCs, 48 colonies were manually picked and plated in duplicated matrigel-coated 96-well plates. DNA was extracted from 96-well plates using QuickExtract DNA Extraction Solution (Epicenter) and genotyping PCR performed using Platinum Taq DNA Polymerase High Fidelity (Thermo Fisher Scientific). Heterozygous edited clones were subjected to a second round of editing using the same method but a different set of sgRNAs to avoid insertions or deletions present at the original sgRNA target site.

2.6.2 SMARCB1 knockdown cell line engineering

Doxycycline-inducible shRNA constructs against SMARCB1 and non-targeting controls were purchased from Dharmacon (SMARTvector Inducible Lentiviral shRNA) (Supplementary table 2.3) and transductions were conducted using Dharmacon Trans-Lentiviral Packaging Kit according to kit protocol. After selection with puromycin, individual clones were generated by plating 1-2 $\times 10^4$ cells in a Matrigel-coated 10 cm tissue culture dish and allowing visible colonies to form. 20-24 clones were picked and screened for SMARCB1 knockdown by quantitative real-time PCR. Top five clones were pooled to obtain a highly efficient knockdown. Of three shRNA constructs tested, only one was capable of efficient SMARCB1 knockdown (sh905).

For CRISPRi experiments, CRISPRi Gen1C cell line (46) was transduced with several guide RNAs targeting the SMARCB1 TSS region or 5' UTR (Supplementary table 2.3) and selected with blasticidin for guide RNA expression. After selection, individual clones were generated by plating 1-2 $\times 10^4$ cells in a Matrigel-coated 10 cm tissue culture dish and allowing visible colonies to form. 20-24 clones were picked and screened for SMARCB1 knockdown by quantitative real-time PCR. Top five clones were pooled to obtain a highly efficient knockdown. Of six sgRNA constructs tested, only one was capable of efficient SMARCB1 knockdown (UTR1).

2.7 Supplementary Tables

Table 2.1. CRISPR-Cas9 sgRNA target sequences

sgRNA	SMARCB1 target site	Target sequence
Ex1-1	Exon 1	CGAAGCCGGAAGGCGAAATG
Ex1-2	Exon1	GCGAGGGATCAGGAGGGCTG
Ex2	Exon 2	GAGAACCTCGGAACATACGG
Ex9-1	Exon 9	GCGCCATCCTGAGGATCGGG
Ex9-2	Exon 9	GCCAGAAGATGGAGGAGAGG
In1-1	Intron 1	GGCCTGGGCAGATGCCTGAG
In1-2	Intron 1	TGCCGAAAGCGTGGCGCCTG
In2-1	Intron 2	GTCGGGCAGGGAGCATCCCG
In2-2	Intron 2	TGCCTGGAGTGCTCACAGGG

Table 2.2. SMARCB1 PCR primers

Primer	Product detection	Primer sequence
Exon 1F	Full-gene deletion/Exon 1 WT	GAAGTCCTCTACACCACGAC
Exon 1R	Exon 1 WT	TCCTCCAGCTGGAACTTCAC
Exon 9R	Full-gene deletion	GGGCTCAACAAATGGAATGTG
Intron 1F	Exon 2 deletion/Exon 2 WT	GTGCCAGAGATCCTTAGTCC
Intron 2R	Exon 2 deletion/Exon 2 WT	CTGACAGTGGACCACCAATG

Table 2.3. shRNA and CRISPRi target sites

Knockdown construct	SMARCB1 target site	Target sequence
sh905	Exon 6	GTGACGATCTGGATTTGAA
sh658	Exon 7	CATACAGCATCCGGGGACA
sh740	Exon 2	CCGTATGTTCCGAGGTTCT
CRISPRi UTR1	UTR	CGGGCTGCGAGGGATCAGGA
CRISPRi TSS1	TSS	GGAGAAAGAGAAATTAGTCG
CRISPRi UTR2	UTR	CGAAGCCGGAAGGCGAAATG
CRISPRi TSS2	TSS	TGGCTCCTTTAAGGGGTCCG
CRISPRi TSS3	TSS	CCGGCCTTTTGTTTGAGCGG
CRISPRi TSS4	TSS	CGCGCCGCCGCTCAAACAAA

2.8 Acknowledgements

While the majority of the material in Chapter 2 has not been published and will not be submitted for publication, sections 2.5 and 2.6 contain portions of material as it appears in Parisian AD, Koga T, Miki S, Johann PD, Kool M, Crawford JR, Furnari FB (2020). ”SMARCB1 loss interacts with neuronal differentiation state to block maturation and impact cell stability.” Genes & Development. The dissertation author is the primary author of this paper.

The authors would like to thank Dr. Bruce Conklin for providing CRISPR interference cell lines and constructs for use in these experiments. I would also like to thank Dr. Tomoyuki Koga for his invaluable assistance and instruction in the implementation of CRISPR-Cas9 editing in an iPSC system.

This work was supported by Padres Pedal the Cause/RADY grant (PTC2017), the National Institute of General Medical Sciences T32GM008666 (A.P.), and the National Institute of Neurological Diseases and Stroke R01-NS080939 (F.F.).

Chapter 3

Interrogating interactions between SMARCB1 and neural differentiation state

3.1 Introduction

As has previously been discussed, the BAF complex has been shown to play important roles in a wide range of developmental processes (32, 33, 35, 36, 48). This is likely due to the widespread remodeling of chromatin architecture which occurs during development. A large portion of the genome has been shown to switch between active and inactive chromatin states during lineage specification (49). This means that the epigenetic landscape (including chromatin state, histone profiles and DNA methylation) can vary dramatically between cells of different lineages or cells at different stages of differentiation. Because SMARCB1 is a subunit of a chromatin remodeling complex, we were curious whether the effects of SMARCB1 loss might vary at different stages of cellular differentiation. If so, this could explain why loss of function mutations in SMARCB1 can have such a dramatic effect on cellular transformation in the case of pediatric ATRT and MRT but are rarely observed in adult tumors. There may be a particular cell type or epigenetic landscape which is particularly sensitive to the effects of SMARCB1 loss, and in which loss of function leads to tumorigenesis. It is even possible that an interaction could take place between the timing of SMARCB1 loss and the transformative epigenetic changes which

occur during the process of cellular differentiation.

3.2 SMARCB1 loss causes differential phenotypes in pluripotent and committed cell types

To interrogate possible interactions between SMARCB1 loss and cellular differentiation state, we generated a doxycycline-inducible SMARCB1 loss of function system in an iPSC line using an inducible shRNA construct targeting SMARCB1 (Figure 3.1A, S3.1A). To rule out the possibility that any observed effects could be due to shRNA off-target effects on genes other than SMARCB1, a doxycycline-inducible SMARCB1 re-expression vector was engineered with either three (m3) or six (m6) silent mutations in the shRNA target sequence (Figure 3.1B, S3.1A). Treatment of this cell line with doxycycline resulted in rapid reduction of SMARCB1 transcript and protein levels (Figure 3.1C,D), both of which were successfully rescued in the presence of re-expression vectors. With this inducible system, SMARCB1 loss could be initiated at various stages of differentiation to observe the interplay between cell state and the effects of SMARCB1 loss. After initial doxycycline induction at the iPSC state, it was observed that prolonged induction of SMARCB1 loss resulted in a pronounced cell death phenotype in shSMARCB1 iPSCs (Figure 3.1E,F) but not in control iPSCs engineered with a non-targeting shRNA. Beginning three days post-doxycycline induction, a pronounced decrease in growth rate was observed (Figure 3.1G) along with an increase in cell death as measured by cell cycle assay, which showed an increase in Sub-G phase dead and dying cells (Figure 3.1F). This SMARCB1-induced cell death phenotype is consistent with mouse model data showing embryonic lethality of SMARCB1 knockout mice (11, 40), but has not been previously demonstrated in human cells. Cell death induced by SMARCB1 loss was replicated in a separate doxycycline-inducible SMARCB1 knockdown iPSC cell line utilizing the CRISPR interference method of transcription repression described in Chapter 2 (Figure 3.2A-E). However, this system proved to be less stable than the shRNA method and was subject to silencing during differentiation. For this reason, all

differentiation experiments were conducted using the shRNA knockdown method with rescue vector. To investigate whether the effects of SMARCB1 loss might vary with differentiation state, iPSCs were differentiated into neural progenitor cells (NPCs) according to the protocol described by Reinhardt et al. (50) (Figure S3.1B) prior to exposure to doxycycline. Cells were induced with doxycycline for 5 days and monitored for changes in morphology or growth rate. In contrast to the iPSCs, SMARCB1 knockdown NPCs tolerated the loss and displayed no changes in growth rate or morphology (Figure 3.1E,H), even with extended doxycycline treatment (data not shown) and a similar level of knockdown as observed in the iPSCs (Figure S3.1C). SMARCB1 knockdown NPCs displayed changes in expression of BAF complex subunits similar to those observed in SMARCB1-deficient rhabdoid cell lines and reductions in BAF complex stability (Figure S3.1D) consistent with those observed in the literature with ATRT cell lines (24), suggesting that shRNA knockdown of SMARCB1 has a similar molecular effect to SMARCB1 loss occurring through genomic deletion.

Figure 3.1. Development of an inducible SMARCB1 knockdown system reveals that SMARCB1 loss causes lethality in pluripotent cells but not neural progenitors. (A) Schematic representation of doxycycline-inducible SMARCB1 shRNA construct, which was stably transduced into induced pluripotent stem cells (iPSCs). (B) Schematic representation of doxycycline-inducible SMARCB1 rescue construct, which was stably transduced into shSMARCB1 iPSCs to rescue SMARCB1 knockdown. Efficacy of shSMARCB1 and rescue vector was tested in iPSCs after 3 days of doxycycline induction using (C) qRT-PCR to measure SMARCB1 transcript levels and standard deviation relative to control mean, or (D) western blot to measure SMARCB1 protein levels. (E) Phase contrast images at 4X magnification of SMARCB1 knockdown iPSCs and NPCs after 5 days of doxycycline induction. (F) Cell cycle assay of 5 day SMARCB1 knockdown iPSCs. Above, FACS readout of PI stained cellular DNA content and corresponding phases of the cell cycle. Numbers indicate percentage of total in each phase. Below, table of percentage differences and 95% confidence interval between control and knockdown at each cell cycle stage. Gold indicates statistically significant differences with 8 replicates. Growth of (G) iPSCs and (H) NPCs was also assessed with doxycycline induction beginning at Day 0 of assay.

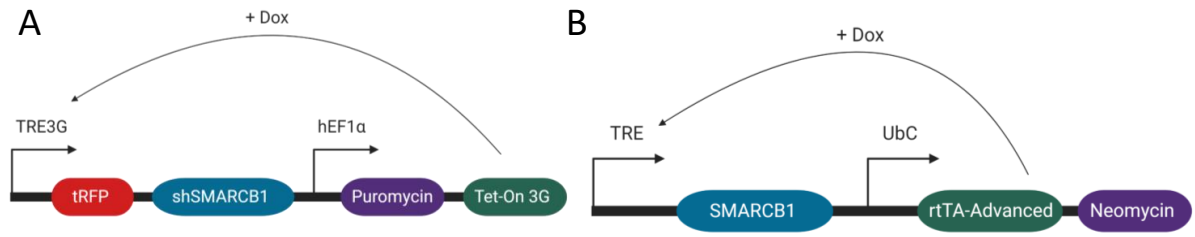

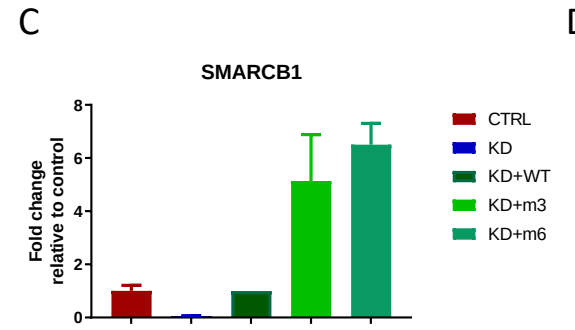

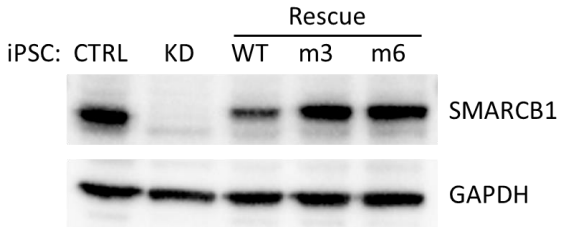

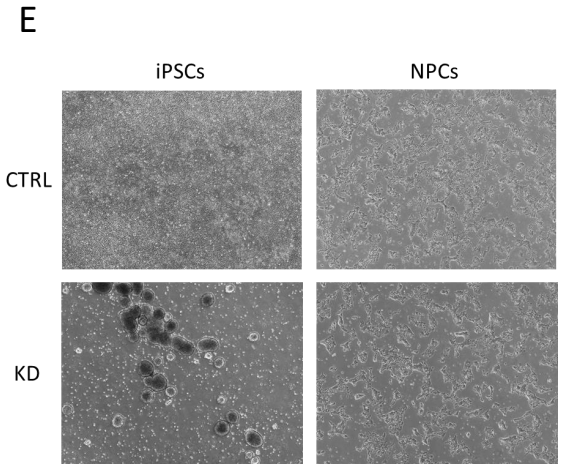

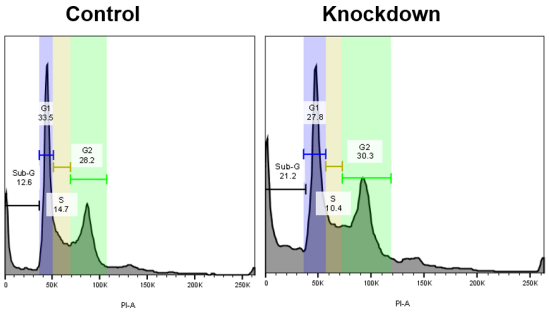

Cell Cycle Phase	95% CI of Difference	P value
G1	-5.413 ± 5.99	P < 0.05
G2/M	0.2250 ± 5.99	P > 0.05
S	-2.787 ± 5.99	P > 0.05
Sub-G	7.975 ± 5.99	P<0.001

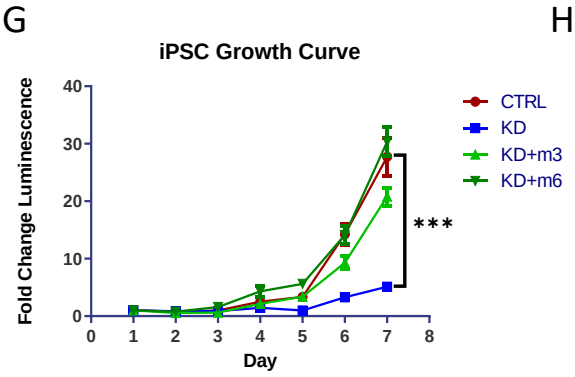

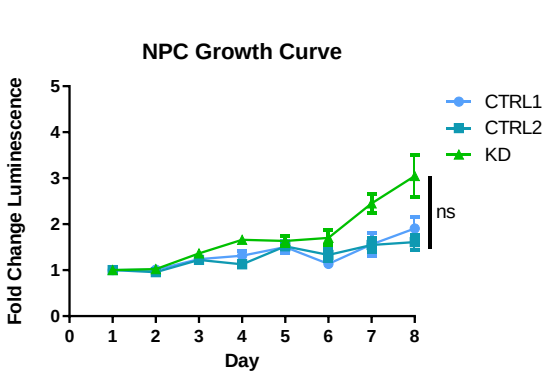

Figure 3.2. SMARCB1 knockdown using CRISPR interference shows similar phenotypes and growth effects to shRNA knockdown in iPSCs. (A) Brightfield images at 2X magnification of cell morphology in CRISPRi control and SMARCB1 knockdown iPSCs after 8 days of doxycycline induction. (B) ATPlite growth curve showing CRISPRi control and SMARCB1 knockdown iPSCs in the presence of doxycycline. * indicates p-value of final timepoint < 0.05. (C) Cell cycle assay of CRISPRi control and SMARCB1 knockdown iPSCs. Left, FACS readout of PI stained cellular DNA content and corresponding phases of the cell cycle. Numbers indicate percentage of total in each stage. Right, table of percentage differences and 95% confidence interval between control and knockdown at each cell cycle phase. Gold indicates statistically significant differences with 8 replicates. (D) Volcano plot of SMARCB1 knockdown CRISPRi iPSC RNA sequencing data relative to control. Statistically significant differences are highlighted in teal. (E) Diagram showing overlap of genes differentially expressed in SMARCB1 knockdown cells relative to control in shRNA iPSCs, CRISPRi iPSCs and shRNA NPCs. Greatest overlap is observed between shRNA and CRISPRi iPSCs.

A

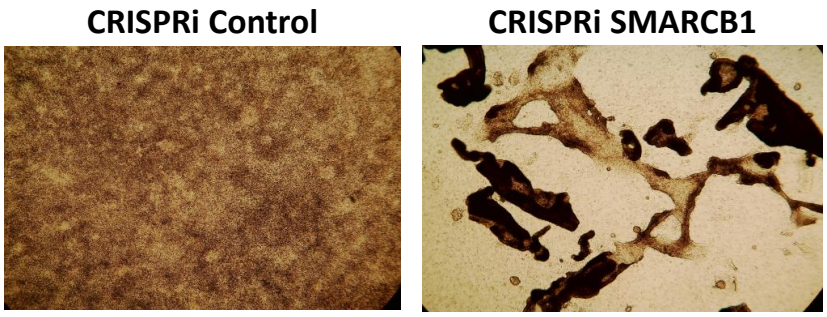

B

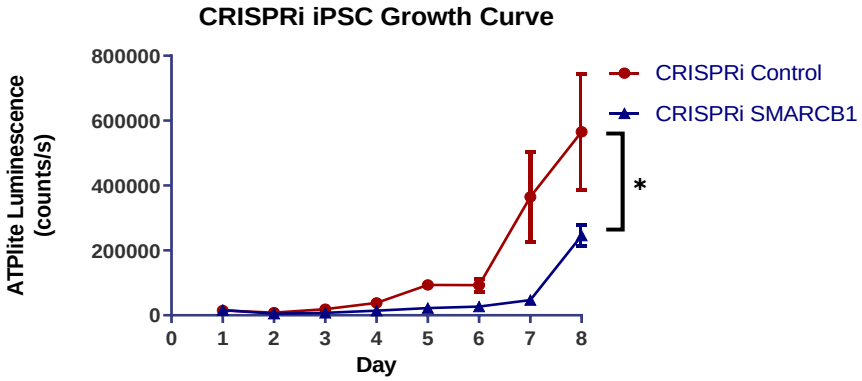

C

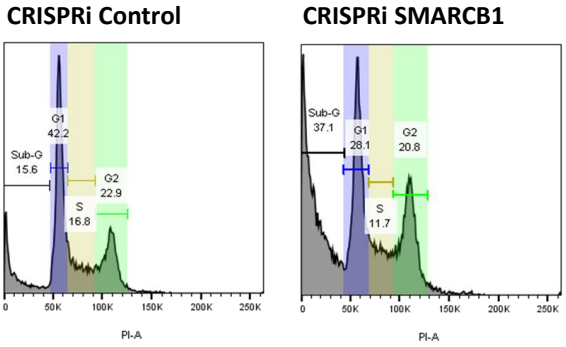

Cell Cycle Phase	95% CI of Difference	P value
G1	-13.90 ± 9.68	P<0.001
G2/M	-9.233 ± 9.68	P < 0.05
S	-0.5467 ± 9.68	P > 0.05
Sub-G	23.57 ± 9.68	P<0.001

D

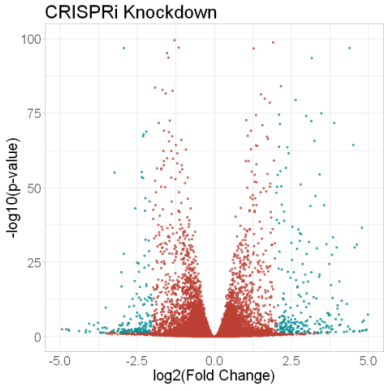

E

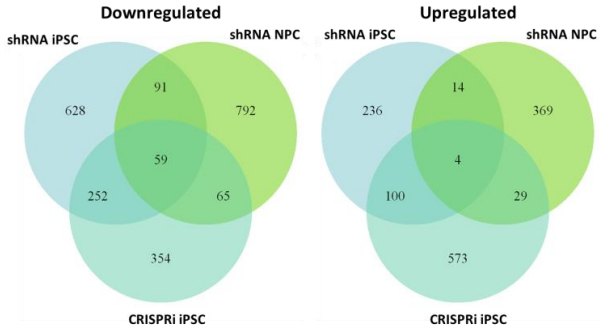

To identify transcriptional differences underlying these contrasting phenotypes, we conducted RNA sequencing on control and SMARCB1 knockdown iPSCs and NPCs. In both cell types, more downregulated genes were observed in SMARCB1 knockdown cells than upregulated genes (Figure 3.2D,E, 3.3A). This is consistent with the previously described mechanism for epigenetic and transcriptional changes underlying ATRT, in which loss of SMARCB1 leads to a decrease in BAF complex activity and a corresponding decrease in H3K27Ac active histone marks, along with altered activity of the polycomb repressive complex 2 (PRC2) (22, 25, 38, 51). Comparison of the genes differentially expressed by SMARCB1 loss in the two cell types revealed very little overlap between knockdown NPCs and iPSCs (Figure 3.3B), suggesting that the downstream targets of SMARCB1 can vary substantially based on cellular context. Gene ontology analysis of the dysregulated genes show similarities in the classes of genes altered by SMARCB1 loss in the two cell types, including genes associated with neural development, cellular proliferation and cellular adhesion (Figure 3.3C,D). However, many of these shared genes were altered in opposite directions in iPSCs and NPCs, both on the ontology level (Figure 3.3E) and on the individual gene level (Figure 3.3F). About a quarter of genes which were dysregulated in both iPSCs and NPCs were upregulated in one cell type but downregulated in the other. This unexpected result suggests that the transcriptional effects of SMARCB1 loss can vary dramatically in different epigenetic environments, even leading to opposite phenotypic and transcriptional effects, and explains the very different growth phenotypes observed in knockdown iPSCs and NPCs. These results, along with the established role of the BAF complex in developmental processes (32, 34, 35), lead us to believe that SMARCB1 loss might also have dramatic impacts on cellular differentiation processes, potentially highlighting an interplay between differentiation state and ATRT tumorigenesis.

Figure 3.3. SMARCB1 loss leads to differing transcriptional effects at defined stages of differentiation. RNA sequencing was conducted on SMARCB1 knockdown and shControl iPSCs and NPCs. (A) Volcano plot of genes differentially expressed in SMARCB1 knockdown cells relative to controls in each cell type. (B) Overlap of genes differentially expressed in SMARCB1 knockdown iPSCs and NPCs relative to controls. (C, D) Gene ontology networks for differentially expressed genes in (C) iPSCs and (D) NPCs. Dots represent statistically significant gene ontology terms, clustered based on overlap of the genes contained in each term. Dot size indicates the number of genes included in each term and darker color corresponds to smaller adjusted p-value. Labels indicate the main process making up each cluster. (E) Table comparing shared gene ontology results and direction of alteration between SMARCB1 knockdown iPSCs and NPCs. q-value was obtained using the Benjamini-Hochberg adjustment for multiple comparisons. (F) Heatmap showing genes which are differentially expressed in both iPSCs and NPCs. Boxes indicate regions which are altered in opposite directions between iPSCs and NPCs. Overall, 62 out of 230 overlapping genes (27%) were altered in opposite directions between the two cell types.

A

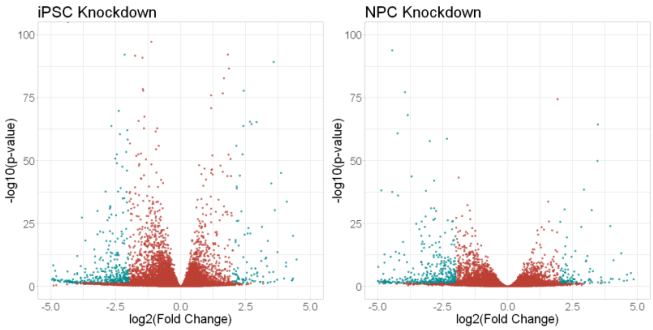

B

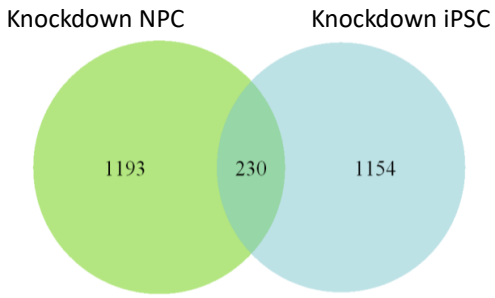

C

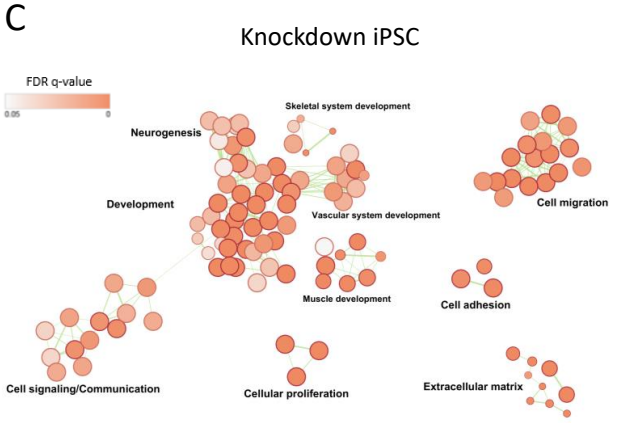

D

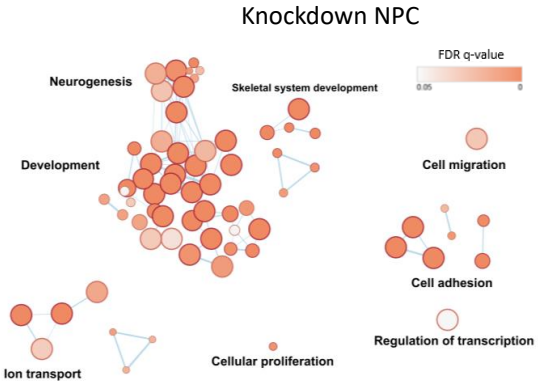

E

Shared: Same direction	Direction and q-value iPSC/ NPC	Shared: Opposite direction	Direction and q-value iPSC/ NPC
Regulation of ion transport	Down $5x10^{-8}$/ $8x10^{-7}$	Positive regulation of cell proliferation	Down $1x10^{-6}$/ Up $7x10^{-5}$
Nervous system development	Both	Extracellular matrix organization	Down $2x10^{-14}$/ Up $2x10^{-2}$
		Cell adhesion	Down $2x10^{-14}$/ Up $1x10^{-2}$
		Negative regulation of programmed cell death	Down $1x10^{-2}$/ Up $1x10^{-2}$

F

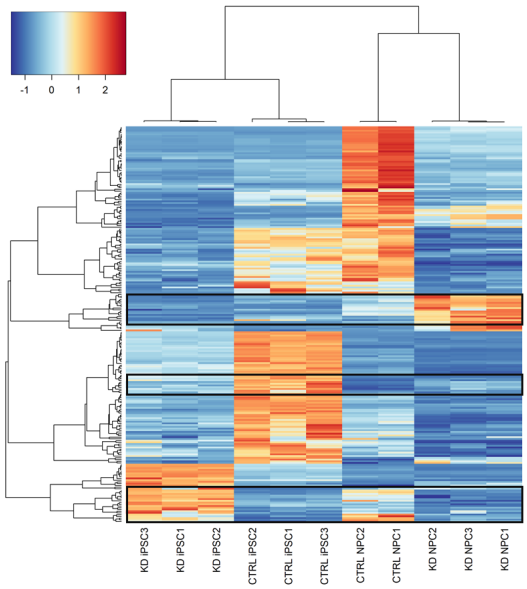

3.3 Neural development without SMARCB1 leads to defects in neuron formation in an organoid model

To assess the effect of SMARCB1 loss on neural differentiation, we utilized a cerebral organoid model of neural development (52) (Figure 3.4A). Because this protocol results in the formation of multiple regional identities without selecting for specific neural cell types (53), the model allows a relatively unbiased assessment of the impact of SMARCB1 loss on the neural developmental process. shControl or shSMARCB1 iPSCs were induced to form cerebral organoids with doxycycline induction beginning at various time points through the protocol and assessed for changes in expression of various neural marker genes (Figure S3.2A). While no obvious changes were observed in markers of pluripotency or neural progenitor formation (Nanog, Pax6), decreases were observed in markers of neuronal commitment and maturation (Dcx, visible trend in Map2), especially with earlier doxycycline induction. It was also observed that these early knockdown organoids demonstrated morphological differences relative to the control during expansion and early maturation phases of the protocol (Figure 3.4B). Knockdown organoids were defective for the outward expansion of neuroepithelium (53) into the surrounding matrix typically observed after Matrigel embedding at Day 7 of the differentiation protocol, suggestive of a defect in normal cell differentiation. These results imply that there is a window early in development where cells are especially sensitive to the effects of SMARCB1 loss.

To better assess the impact of early-stage SMARCB1 loss on neural differentiation we conducted droplet-based single-cell RNA sequencing (scRNA-seq) on three control and three SMARCB1 knockdown organoids at Day 20 of the differentiation protocol, when morphological differences were apparent. These six organoids (Figure S3.2B) were aligned and clustered using canonical correlation analysis (54) in order to compare numbers of neural cell types between control and knockdown organoids. Cluster analysis resulted in 15 distinct clusters (Figure 3.4C, Figure S3.2C-D), one of which was excluded for containing less than 100 cells. All but one of these remaining clusters (cluster 10) contained a similar distribution of cells

across replicate organoids (Figure S3.2B). Organoids had similar distributions of UMI counts and detected genes (Figure S3.2E), and SMARCB1 knockdown organoids displayed loss of SMARCB1 transcript in nearly all cells analyzed (Figure S3.2F). Clusters were analyzed for expression of several neural development marker genes to identify corresponding cell types (Figure 3.5A-F) and Slingshot pseudotime analysis (55) was performed to identify differentiation trajectories across clusters (Figure 3.4C). This analysis revealed a mix of clusters representing neural progenitors, positive for markers such as Sox2, Pax6, and Hes1 (Figure 3.5A, C, D), and various stages of neuronal differentiation including intermediate progenitors (Figure 3.5E), immature neurons, and more mature neurons (Figure 3.5F). Within the progenitor clusters, some seemed to represent neuroepithelial cells and some radial glia (Figure 3.5B, D), while others were negative for markers of either of these cell types and may represent progenitors of a distinct lineage (clusters 1, 10, 12). Other clusters were defined by aspects of cell state such as cell cycle stage or apoptosis (Figure 3.5B) rather than cell type. Grouping together the identifiable clusters representing neuroepithelial progenitors (cluster 4) and radial glia-like cells (clusters 0, 7, 11), intermediate progenitors (clusters 3, 13), and committed neurons (clusters 2, 5, 14) (Figure 3.4D), the number of cells in each group were quantified in both control and SMARCB1 knockdown organoids. The number of neuron-associated clusters was substantially lower in SMARCB1 knockdown organoids ($p < 0.001$) than controls (Figure 3.4D, Figure S3.2D) and the expression of individual neuronal markers was lower in knockdown organoids (Figure 3.5G), suggesting that the knockdown might be causing a differentiation block and preventing cells from achieving a neuronal cell fate. Although no differences were observed in the number of neuroepithelial or radial glial progenitors, some apparent increases (although not statistically significant to $p < 0.05$ with current number of replicates), spread across progenitor clusters 1, 12 and 10 (Figure 3.4D, S3.2D) suggest that SMARCB1 loss might lead to a shift in the lineage preference of cells during differentiation while contributing towards a preference for less differentiated cell types.

Figure 3.4. SMARCB1 loss during cerebral organoid development leads to neural differentiation defects. Cerebral organoids were formed from shSMARCB1 and shControl iPSCs in the presence of doxycycline from Day 0 of differentiation protocol. (A) Schematic showing stages of organoid generation from iPSCs. (B) At day 20 of the protocol (10 days of maturation), organoids were examined for morphology and presence of neuroepithelial expansion (black arrows) at 4X magnification. White arrow indicates absence of neuroepithelial expansion. (C) Single-cell RNA sequencing was conducted on three Day 20 control and SMARCB1 knockdown organoids using droplet-based scRNA-seq methodology. Canonical correlation analysis was conducted on combined single-cell data and displayed on a tSNE graph. Clustering and pseudotime analysis was conducted on the combined data to identify variability in cell types and lineages within the organoids. Fifteen clusters were identified, of which cluster 15 was excluded from analysis due to its small size. (D) Left, clusters were analyzed for expression of neural differentiation markers and grouped together by cell type where possible. Clusters not matched to a particular cell type were left unnamed. Right, mean with standard deviation of the number of each cell type in control and knockdown organoids. Statistical comparisons were conducted using two-way ANOVA with Sidak multiple comparisons test. *** indicates adjusted p-value < 0.001. (E) Venn diagram of the overlap across cell types of genes differentially expressed in SMARCB1 knockdown organoids relative to control organoids. (F) Tables showing top gene ontology results from genes differentially expressed in SMARCB1 knockdown organoids relative to controls relative to a list of all expressed genes in progenitor cells, left, and neurons, right. Ontologies highlighted in gold are similarly altered in both cell types.

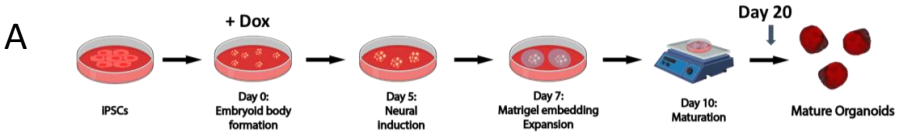

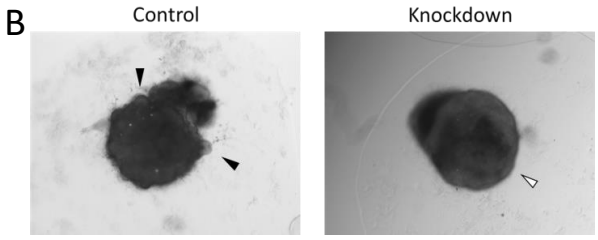

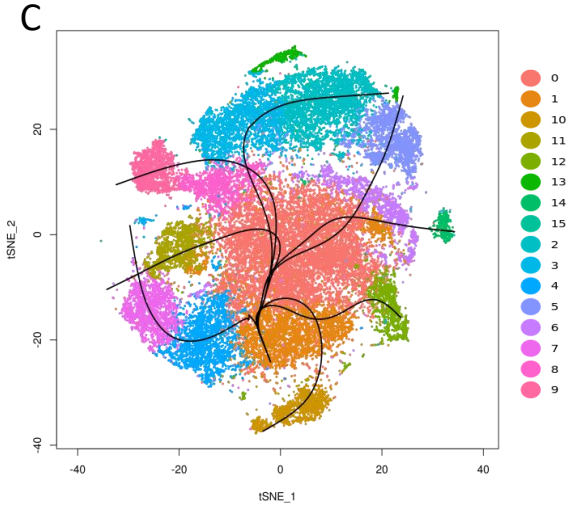

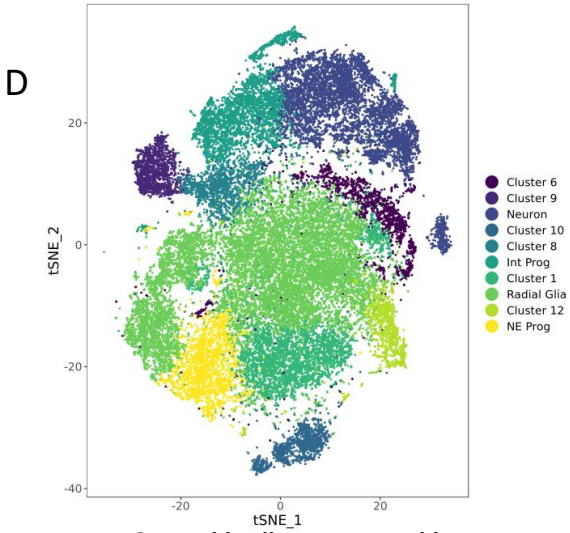

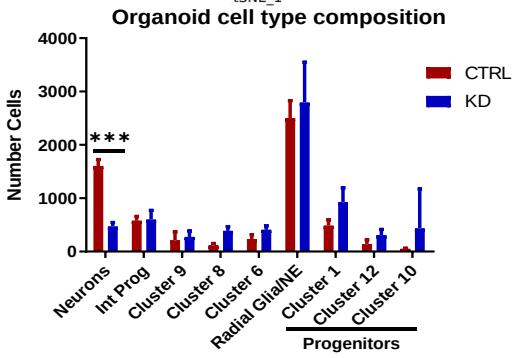

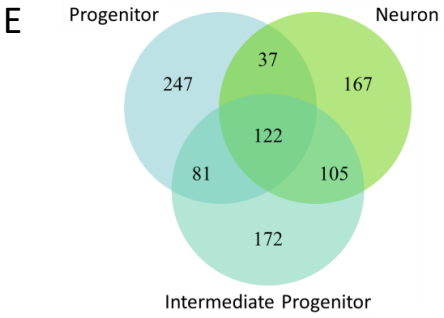

F

Gene Ontology: Progenitors	Direction in knockdown	FDR q-value
Nervous system development	Down	
Negative regulation of cell death	Up	2.4×10^{-3}
Canonical glycolysis	Up	4.3×10^{-5}
Regulation of transcription by RNA polymerase II	Down	5.5×10^{-7}
Positive regulation of cell migration	Up	6.6×10^{-3}
Extracellular matrix organization	Up	3.8×10^{-3}
Wnt signaling pathway	Down	2.3×10^{-2}
BMP signaling pathway	Down	1.8×10^{-2}

Gene Ontology: Neurons	Direction in knockdown	FDR q-value
Positive regulation of neuron differentiation	Down	1.5×10^{-2}
Synapse organization	Down	2.8×10^{-2}
Positive regulation of cell death	Up	4.7×10^{-4}
Regulation of RNA splicing	Down	1.2×10^{-2}
Canonical glycolysis	Up	7.9×10^{-6}
Regulation of transcription by RNA polymerase II	Down	4.2×10^{-2}

Differences in the gene expression changes caused by SMARCB1 loss across cell types within the organoids highlight the effects of SMARCB1 loss on differentiation as well as further demonstrating that the transcriptional effects of SMARCB1 loss vary with cell state. For differential expression analysis, related clusters were combined to form larger groups representing different stages of neural differentiation: neural progenitor cells (combining neuroepithelial progenitors, radial glia, and progenitor clusters 1 and 12), intermediate neuronal progenitors, and committed neurons. For each cell type, differential expression analysis was conducted comparing cells of that type in the control and knockdown organoids. A similar number of genes were significantly dysregulated in each cell type, but only about a quarter of these were dysregulated in all three cell types (Figure 3.4E). In addition, the number of overlapping genes was greater between more closely related cell types (progenitors and intermediates or intermediates and neurons) than between the more distantly related progenitors and committed neurons. This suggests that there may be a spectrum of transcriptional changes occurring without SMARCB1 that varies throughout the developmental process and has different effects on cells at different stages of cellular differentiation. Gene ontology analysis of dysregulated genes in neural progenitors and neurons showed that different biological processes were affected in the two cell types (Figure 3.4F). While canonical glycolysis was upregulated in both cell types and genes associated with both neural development and transcriptional regulation were downregulated, cell death processes were altered in opposite directions. In addition, neural progenitors had additional changes in pathways associated with cellular migration, extracellular matrix organization, Wnt signaling and BMP signaling which were not observed in the more differentiated cells. These differences in transcriptional state illustrate how SMARCB1 loss could lead to distinct cellular phenotypes depending on the cellular epigenetic landscape.

Figure 3.5. Cell type determination of clusters in organoid single-cell RNA-seq data. (A) tSNE plots of overlaid control and SMARCB1 knockdown organoids colored for expression of SMARCB1 and various neural marker genes ranging from those common in less differentiated cells (top) to those common in more differentiated neurons (bottom). (B) Heatmap of top 10 differentially expressed genes in each cluster after a differential expression analysis comparing all clusters. Yellow indicates higher expression and purple/black indicates lower expression. Labels on right indicate cell types or processes enriched in that group of genes. (C) Violin plots showing expression of neural progenitor markers Sox2 and Pax6 across organoid clusters. (D) Violin plots showing expression of intermediate neuronal progenitor markers EOMES and NHLH1 across organoid clusters. (E) Violin plots showing expression of neuronal markers DCX and STMN2 across organoid clusters. (F) Violin plots showing expression of radial glia markers Hes1 and Hes5 across organoid clusters. (G) Above, tSNE plots of control (lower subplot) and knockdown (upper subplot) organoids colored for level of expression of neuron markers MAP2, STMN2, TUBB2A, SYT1, SYP, and NRXN1. Below, violin plots of neuron markers MAP2 and STMN2 in control and knockdown organoids. Knockdown organoids show a lower amount of expression for neuronal markers than control organoids.

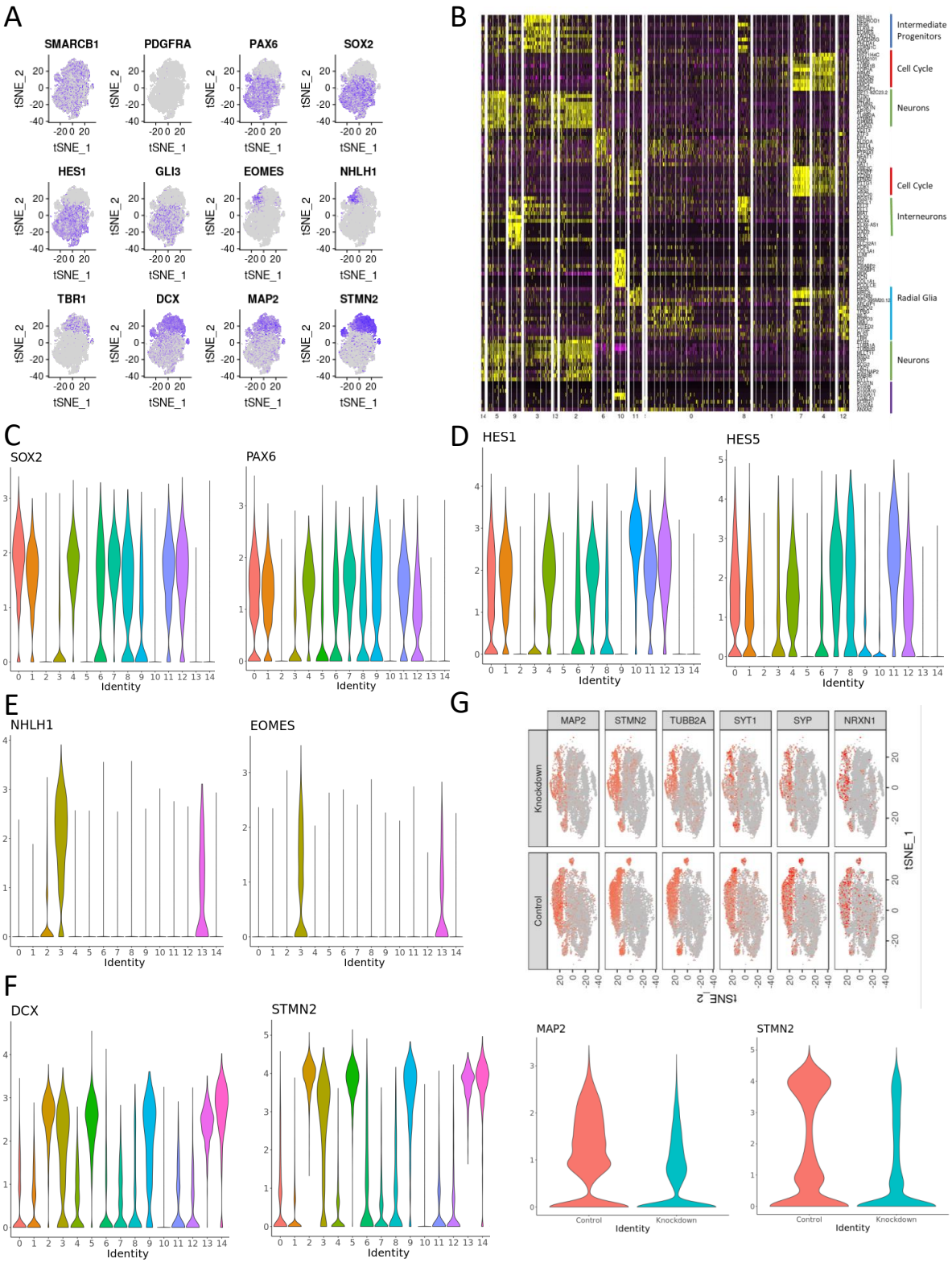
A
SMARCB1
PDGFRA
PAX6
SOX2
HES1
GLI3
EOMES
NHLH1
TBR1
DCX
MAP2
STMN2
tSNE_1
tSNE_2
B
Intermediate Progenitors
Cell Cycle
Neurons
Cell Cycle
Interneurons
Radial Glia
Neurons
C
SOX2
PAX6
Identity
D
HES1
HES5
Identity
E
NHLH1
EOMES
Identity
F
DCX
STMN2
Identity
G
MAP2
STMN2
TUBB2A
SYT1
SYP
NRXN1
Knockdown
Control
tSNE_1
tSNE_2
MAP2
STMN2
Control
Knockdown
Identity

3.4 Perspectives and conclusions

Through the generation of a doxycycline-inducible SMARCB1 knockdown human iPSC line, we have been able to provide novel insights into the relationship between SMARCB1 loss and neural development. We have shown directly that both cellular growth phenotypes and transcriptional changes resulting from SMARCB1 loss can vary substantially between pluripotent cells and committed neural lineage cells. We have demonstrated that SMARCB1 loss at the pluripotent state leads to cell lethality, an observation which provides insight into embryonic lethality phenotypes observed in SMARCB1 knockout mouse models (11, 40). And we have utilized our cell line to observe the morphological and transcriptional effects of SMARCB1 loss on the process of neural development as recapitulated in an organoid model. We observed that loss of SMARCB1 expression throughout neural development results in differentiation defects and impairs the ability of neuronal cells to mature appropriately. This discovery may provide insight into mechanisms which contribute to ATRT tumorigenesis, an idea which will be discussed further in additional chapters.

3.5 Methods

3.5.1 Pluripotent stem cell culture and neural differentiations

Human induced pluripotent stem cell (iPSC) line iPS12 was purchased from Cell Applications. This cell line is integration-free and was validated for pluripotency, viability, karyotype normality and normal disease status by Cell Applications. CRISPRi Gen1C and WTC iPS lines were obtained from the Conklin lab at University of California San Francisco. iPSCs were cultured using standard feeder-free conditions with mTESR1 or mTESR Plus medium on Matrigel-coated plates. iPSCs were induced to form neural progenitor cells using a small-molecule based differentiation protocol as described in Reinhardt et al. (50), using combined small-molecule inhibition of BMP and TGF β signaling along with WNT and SHH pathway stimulation. Neuron differentiations were also conducted as described in Reinhardt et al. for

peripheral neurons (50), starting from NPCs of 3-6 passages in smNPC maintenance medium (N2B27 medium + CHIR + PMA). Neurons were harvested after two weeks in neuronal maturation medium (N2B27 medium + dbcAMP + TGF-b3 + BDNF + GDNF). Both neural progenitor and neuron differentiations were conducted under 0.5 μg/mL puromycin to prevent loss of shRNA expression. Rescue cell lines were differentiated in the presence of 0.5 μg/mL puromycin and 100 μg/mL G418. When needed, doxycycline was applied at a 1 μg/mL concentration for all experiments.

3.5.2 Organoid development and culture

Organoids were generated using the STEMdiff Cerebral Organoid Kit from Stemcell Technologies (Cat. 08570), which is based on the Lancaster et al.(52) protocol for cerebral organoid formation and development. Organoids were developed in the presence of 0.5 μg/mL puromycin and 1 μg/mL doxycycline. Organoids were matured for 10-50 days in Maturation Medium (Day 10 of protocol). Organoids used for single-cell RNA-seq were matured for 10 days to look at early-stage commitment and development of neural progenitors.

3.5.3 Growth, cell cycle and cell death assays

For growth assays, 1000-2000 cells/well with 5-10 replicates per cell line were plated on Matrigel-coated black 96-well plates in maintenance medium without antibiotic selection. First timepoint was read within 24 hours of plating for baseline comparison and subsequent readings were performed every 24 hours following. Medium changes were conducted as needed (every 2-3 days) throughout the assay. ATPlite 1step assay kit (PerkinElmer 6016731) was used to estimate cell number. For cell cycle assays, eight replicate doxycycline inductions of 1×10^6 cells were harvested and fixed overnight in 70% ethanol, washed three times with PBS and stained for 30 minutes with 0.5 mL FxCycle PI/RNase Staining Solution (Life Technologies F10797) before quantification with a BD LSR II flow cytometer. Cell cycle percentages were calculated using FlowJo software and the Dean-Jett-Fox model. Doxycycline was added to shRNA iPSCs for 5

days before fixation and to CRISPRi iPSCs for 9 days before fixation.

3.5.4 Western blots and immunoprecipitations

For western blots, cells were lysed in RIPA lysis buffer with proteinase and phosphatase inhibitors. 20 μg lysate was run on an SDS-PAGE gel, transferred at 350 mA over 1.5 hours to EMD Millipore Immobilon-P PVDF membrane, blocked for one hour in 5% BSA, and probed with primary antibody overnight. Membranes were washed with PBS + 0.1% Tween-20, probed for 1-2 hours with secondary HRP-conjugated antibody and exposed using Thermo Scientific SuperSignal West Pico or Femto Chemiluminescent Substrate. For BAF complex immunoprecipitations, nuclear extractions were first performed using Thermo Scientific NE-PER Nuclear and Cytoplasmic Extraction Reagents (78833) according to kit instructions. For immunoprecipitations, 2 μg of BRG1 antibody (Santa Cruz, sc-17796) was incubated for one hour with 20 μL Dynabeads Protein G magnetic beads (Thermo Fisher Scientific, 10004D), washed, then incubated overnight at 4 ith 500 μg of nuclear lysate, washed and prepared for SDS-PAGE. Washes were conducted with either citric or RIPA buffer, as specified. Western blots were run as previously described. Primary antibodies used for western blots were: SMARCB1/BAF47 (mouse, 1:500, BD Biosciences, 612110), GAPDH (rabbit, 1:5000, 2118), HDAC1 (rabbit, 1:1000, Cell Signaling, 2062), SMARCD1 (mouse, 1:1000, Santa Cruz, sc-135843), SMARCC1 (rabbit, 1:1000, Santa Cruz, sc-10756), BRG1 (mouse, 1:1000, Santa Cruz, sc-17796), Nestin (rabbit, 1:1000, EMD Millipore).

3.5.5 Single-cell RNA sequencing preparation and analysis

Three replicate control and knockdown Day 20 organoids (10 days maturation) were collected, washed and incubated for one hour on a 37 C shaker in Accutase + 50 μg/mL DNaseI to aid in generation of a single-cell suspension. Organoids were dissociated by gentle pipetting with a wide-bore pipette after 15 and 45 minutes of incubation. Clumps were removed by filtration through a cell strainer, resuspended in PBS+0.04% BSA, counted and resuspended to a

1.2×10^6 cells/mL concentration. Cell viabilities were 60-80% with a total of 5×10^4 to 2×10^5 cells collected per organoid. Samples were prepared for single-cell RNA sequencing as detailed in the 10X Chromium Single Cell 3' Reagent Kits v2 User Guide. Reagents used included the Chromium Single Cell 3' Library & Gel Bead Kit v2 (PN-120237), Chromium Single Cell A Chip Kit (PN-120236) and Chromium i7 Multiplex Kit (PN-120262). The protocol was followed for a desired 10,000 cells per organoid using 10 cycles of cDNA amplification. Quality control was conducted after cDNA amplification and library construction on a BioAnalyzer TapeStation instrument. Sample libraries were pooled, and shallow sequencing conducted on an Illumina HiSeq4000 to estimate cell numbers and read counts for each sample and a new pool generated to obtain 50000 reads/cell for each sample. Final sequencing was conducted on an Illumina NovaSeq 6000. Analysis of the resulting data was conducted using the Cell Ranger pipeline for counting and aggregation of sequencing reads. Additional analysis was then conducted using the Seurat R toolkit for single cell genomics (54). Cells with a mitochondrial DNA percentage above 0.1 were filtered out of subsequent analysis. Canonical correlation analysis was conducted using variable genes from the control and knockdown conditions, and a tSNE plot of the first 20 aligned subspaces used for visualization. Clusters were generated using a resolution value of 0.6 and the first 20 CCA subspaces, resulting in the identification of 15 clusters, of which cluster 15 was excluded from later analysis due to its small size. Identification of cluster markers, differential expression analysis, and cluster quantifications were all conducted using the Seurat toolkit. Gene ontology analysis of differential expression gene sets was conducted using the Gorilla (56) website in comparison to a background list of expressed genes.

3.6 Supplementary Figures

Figure S 3.1. Doxycycline-inducible SMARCB1 knockdown system efficiently reduces SMARCB1 levels in both iPSCs and NPCs. (A) Table of shRNA sequence and target sequence on SMARCB1, along with sequences of rescue vectors at shSMARCB1 target site. Induced mutations for resistance to shSMARCB1 are shown in red. (B) Above, schematic of NPC differentiation protocol and below, qRT-PCR mean and standard deviation of shControl NPC transcript levels of several markers of pluripotency or NPC differentiation relative to those in undifferentiated iPSCs for two different iPSC cell lines. (C) Western blots of SMARCB1 and GAPDH protein levels in iPSCs (left) in comparison to ATRT cell line BT16 and rhabdoid cell line G401 and (right) in NPCs induced for three days with doxycycline. (D) Immunoblot of BAF complex subunits in shControl and SMARCB1 knockdown NPC and BT16 cell line nuclear lysates and BRG1 immunoprecipitation. BRG1 immunoprecipitations were conducted with both a milder citric buffer wash and the more stringent RIPA buffer to assess differences in complex stability under both conditions. HDAC1 in nuclear lysates serves as loading control.

A

Construct	Sequence	RNA region targeted	SMARCB1 region
shSMARCB1	TTCAAATCCAGATCGTCAC	ORF	Exon 6
shSMARCB1 target site (WT rescue)	GTGACGATCTGGATTTGAA		
shSMARCB1 m3 rescue	GCGATGACCTCGACTTAAA		
shSMARCB1 m6 rescue	GCGATGACCTCGACTTAAA		

B

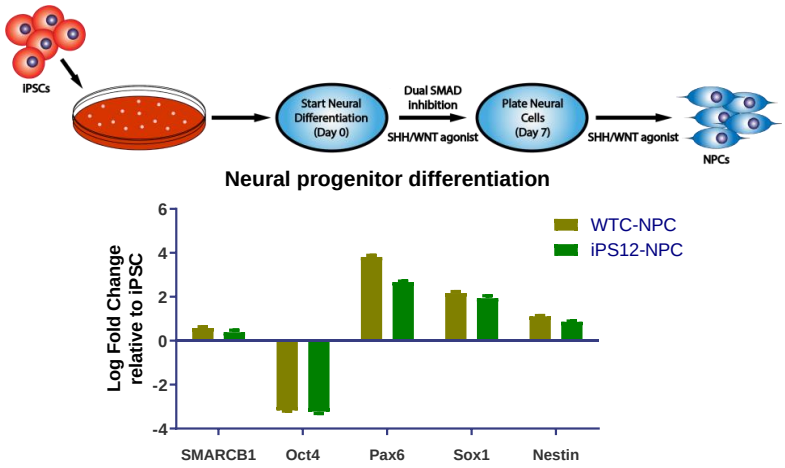

C

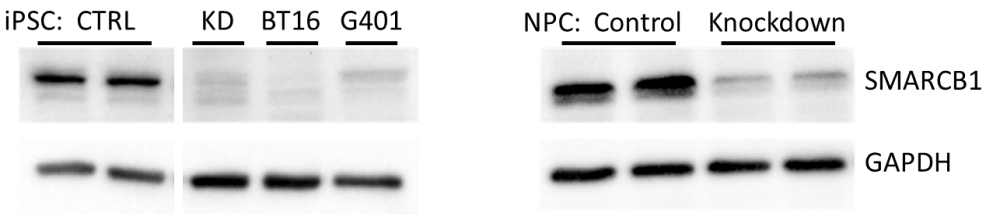

D

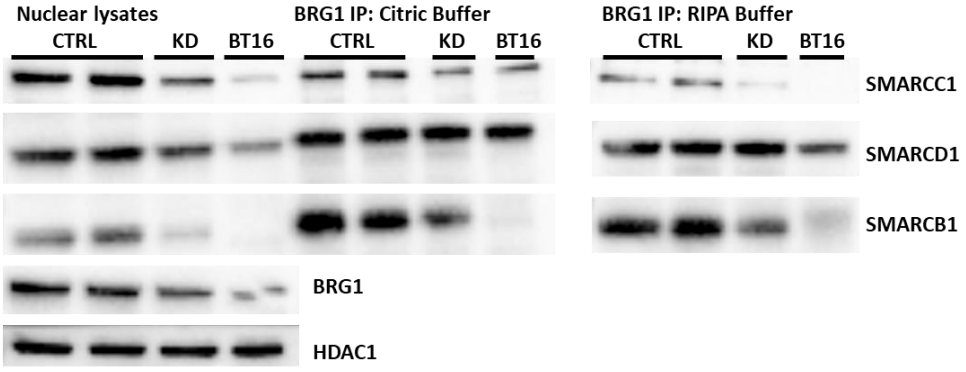

Figure S 3.2. Additional visualizations and metrics of organoid single-cell RNA-seq data. (A) qRT-PCR analysis of SMARCB1 transcript levels and neural development-associated genes in Day 20 organoids with doxycycline induction at various timepoints during the organoid development protocol. Plotted is transcript fold-change relative to GAPDH and standard deviation. Comparisons were conducted using one-way ANOVA with Tukey's multiple comparisons test. *** indicates adjusted p-value < 0.001, ** indicates adjusted p-value < 0.01, * indicates adjusted p-value < 0.05. (B) Overlaid single-cell RNA sequencing data of three control and SMARCB1 knockdown organoids graphed on a tSNE plot, colored by organoid of origin. (C) Phylogenetic tree of organoid clusters. Clusters on the left represent more differentiated neurons or neuronal intermediates, while those on the right represent less differentiated progenitors. (D) Quantification of the mean and standard deviation number of cells in each cluster in control and SMARCB1 knockdown organoids. (E) Graphs of single-cell RNA sequencing UMI counts and gene counts for individual organoids. (F) tSNE plots of control organoids (left) and SMARCB1 knockdown organoids (right) colored by level of SMARCB1 expression.

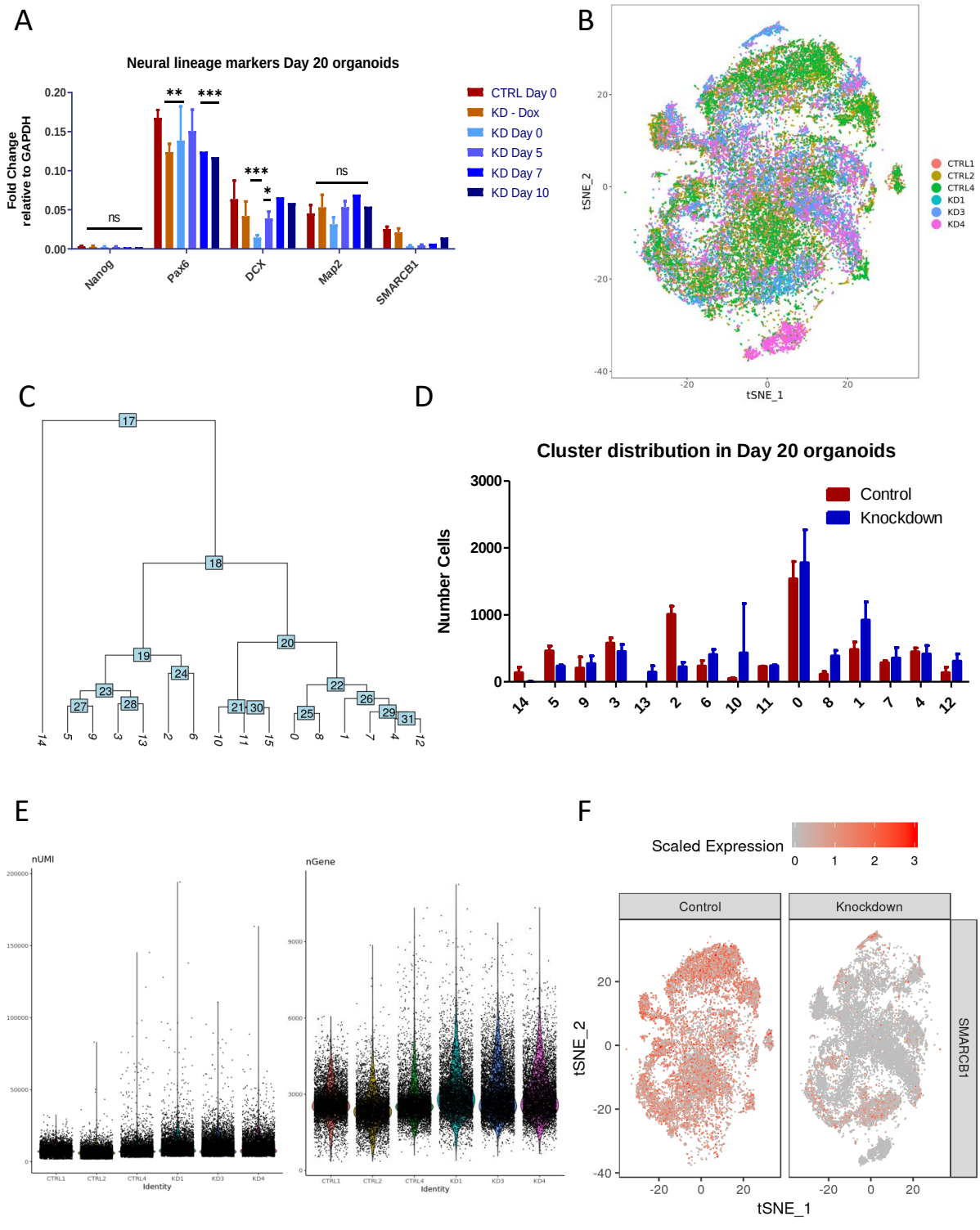
A
Neural lineage markers Day 20 organoids
Fold Change relative to GAPDH
0.20
0.15
0.10
0.05
0.00
**
***
***
*
ns
ns
Nanog
Pax6
DCX
Map2
SMARCB1
CTRL Day 0
KD - Dox
KD Day 0
KD Day 5
KD Day 7
KD Day 10
B
tSNE_2
tSNE_1
CTRL1
CTRL2
CTRL4
KD1
KD3
KD4
C
17
18
19
20
24
23
28
27
22
26
29
31
21
30
25
14
5
9
3
13
2
6
10
11
15
0
8
1
7
4
12
D
Cluster distribution in Day 20 organoids
Number Cells
3000
2000
1000
0
Control
Knockdown
14
5
9
3
13
2
6
10
11
0
8
1
7
4
12
E
nUMI
nGene
Identity
CTRL1
CTRL2
CTRL4
KD1
KD3
KD4
F
Scaled Expression
0
1
2
3
Control
Knockdown
SMARCB1
tSNE_2
tSNE_1

3.7 Acknowledgements

Chapter 3, in full, contains modified material as it appears in Parisian AD, Koga T, Miki S, Johann PD, Kool M, Crawford JR, Furnari FB (2020). ”SMARCB1 loss interacts with neuronal differentiation state to block maturation and impact cell stability.” Genes & Development. The dissertation author is the primary author of this paper.

I would like to thank Dr. Tomoyuki Koga for his assistance with single-cell RNA sequencing sample and library preparations. I would also like to thank Dr. Diana Hargreaves for provision of BAF complex antibodies for use in BAF complex western blots and immunoprecipitation experiments.

This work was supported by Padres Pedal the Cause/RADY grant (PTC2017), the National Institute of General Medical Sciences T32GM008666 (A.P.), and the National Institute of Neurological Diseases and Stroke R01-NS080939 (F.F.).

Chapter 4

Investigating interactions between ATRT tumorigenesis and cellular differentiation state

4.1 Introduction

In addition to their normal roles during development, many BAF complex genes have demonstrated roles as tumor suppressor genes. When taken together, the 20 BAF subunit genes have been shown to be mutated in 19% of all tumor types (21). This speaks to the important genome-wide role of this complex in maintenance of a stable epigenome. Genetic loss-of-function of SMARCB1 in particular has been shown to be both sufficient and necessary for tumorigenesis of atypical teratoid rhabdoid tumors (ATRT) (7, 9, 57), a highly aggressive and early onset pediatric brain tumor. The mutation rate in ATRT is very low (8, 14), with no other consistent recurrent mutations identified. This low number of mutations is consistent with an early age of onset, but also implies that SMARCB1 loss likely leads to tumorigenesis through initiation of epigenetic changes rather than through the combined effect of multiple genetic mutations. While transcriptomic and epigenomic analyses of ATRT samples (13-15, 51) have characterized the epigenetic alterations which take place following SMARCB1 loss, the mechanisms by which SMARCB1 loss leads to these changes and the factors required for SMARCB1 loss to initiate cellular transformation are not well understood. Increased PRC2

binding (22, 38) and skewed SMARCB1-deficient BAF complex binding at super-enhancers (24, 25) have been suggested mechanisms of tumorigenesis due to SMARCB1 loss, but many questions still remain unanswered. The sufficiency of SMARCB1 deletion to drive pediatric tumor growth but lack of SMARCB1 mutation as an exclusive driver mutation in adult cancers, along with the demonstrated role of the BAF complex in development and differentiation leads us to the hypothesis that the ability of SMARCB1 deletion to cause tumorigenesis may be dependent on the epigenetic environment of a particular stage in cellular differentiation.

4.2 SMARCB1 loss during neuronal differentiation leads to a lack of stability among neural progenitors which may contribute to tumorigenesis

To further investigate the effects of SMARCB1 loss on neural differentiation processes and how these might relate to cancer, iPSCs were induced with doxycycline and simultaneously differentiated into neural progenitor cells (Figure 4.1A). Resulting progenitors were cultured for several passages post-differentiation to assess their ability to maintain an NPC state, and it was observed that NPCs differentiated without SMARCB1 were prone to morphology changes 2-5 passages post-differentiation (Figure 4.1A), while control and SMARCB1 rescue NPCs maintained a consistent morphology for up to 10 passages (data not shown). NPCs differentiated without SMARCB1 were also subject to a low-frequency enhancement in growth rate (Figure 4.2A), another indication of a lack of stability in these cells relative to control or rescue NPCs. These cells demonstrated a reduction in levels of neural progenitor marker Nestin (Figure 4.1B) which is prevented by SMARCB1 rescue, implying a defect in differentiation in the absence of SMARCB1, consistent with observed results using the organoid system. Analysis of BAF complex expression levels in NPCs differentiated without SMARCB1 revealed a decrease in levels of nuclear BAF complex subunits ARID1A, BRG1, SMARCC1, and SMARCD1 relative to control NPCs (Figure 4.1C), consistent with what has been observed in SMARCB1 re-expression cell lines (24). However, the level of decrease varied substantially in different

batches of differentiation for the same level of SMARCB1 knockdown (Figure 4.1C), suggesting a stochasticity in the downstream effects of SMARCB1 loss after application of cellular differentiation pressures. RNA-seq of four NPC lines differentiated in the absence of SMARCB1 also revealed a higher transcriptomic variability than was observed in control or rescue cells differentiated with doxycycline or in NPCs subjected to SMARCB1 loss post-differentiation (Figure 4.1D). Correlations within replicates of NPCs differentiated without SMARCB1 were significantly lower than rescue NPCs or NPCs with SMARCB1 knockdown induced at the NPC state. A comparison in the genes dysregulated when SMARCB1 is absent throughout NPC differentiation and those altered with SMARCB1 loss at the NPC state (Figure 4.1E, 4.2B,C) revealed that SMARCB1 loss throughout the differentiation process leads to changes in a wide variety of differentiation-associated pathways ranging from renal development to ossification in addition to the expected neural development-associated genes. Changes in pathways associated with cell death, cellular proliferation and TGF-beta signaling are also observed in genes dysregulated by SMARCB1 loss when it occurs during NPC differentiation. A time course of doxycycline application throughout the NPC differentiation process (Figure 4.2D) verified that more deleterious effects on neural development are observed with earlier induction of SMARCB1 loss.

Figure 4.1. SMARCB1 loss throughout neural differentiation leads to aborted differentiation and a lack of stability in resulting neural progenitor cells. (A) Above, schematic of directed differentiation of iPSCs into neural progenitor cells, with doxycycline induction at Day 0. Below, phase contrast images at 20X magnification of resulting NPC morphology at Day 10-14 of protocol. Cells with abnormal morphology are observed migrating between NPC clusters in cells differentiated without SMARCB1. (B) Western blot showing protein expression of SMARCB1, neural marker Nestin, and control GAPDH in control, SMARCB1 knockdown or rescue NPCs differentiated in the presence of doxycycline. (C) Western blot of BAF complex subunit protein expression in nuclear lysates of NPCs differentiated in the presence of doxycycline. (D) Top, schematic of NPC differentiation with doxycycline induction occurring either at the beginning of the differentiation process (NPC diff.) or at the NPC state (NPC). Middle, Pearson correlation chart comparing transcriptome similarity between control, knockdown or rescue NPCs differentiated with or without doxycycline. Black boxes indicate groups being compared. White corresponds to greater correlation and red to lower correlation. Bottom, mean within group correlation values with standard error of the mean for each group of NPCs. Within group correlations were compared using one-way ANOVA with Tukey's multiple comparisons test. ** indicates adjusted p-value < 0.01. (E) Gene ontology network of top 500 genes which were differentially expressed in NPCs differentiated with SMARCB1 knockdown relative to controls but not in NPCs with knockdown post-differentiation relative to controls. Dots represent statistically significant gene ontology terms, clustered based on overlap of the genes contained in each term. Dot size indicates the number of genes included in each term and darker color corresponds to smaller adjusted p-value. Labels indicate the main process making up each cluster. (F) Top, schematic showing directed neuronal differentiation with doxycycline induction either at Day 0 or at the NPC state. Control and SMARCB1 knockdown neurons differentiated in this manner were assessed for neuronal maturation efficacy by FACS analysis for neuronal surface marker NCAM1. Bottom, mean and standard deviation percentages of NCAM positive cells in post-differentiation neurons. Comparisons between groups were conducted by one-way ANOVA with Tukey's multiple comparisons test. * indicates p-value < 0.05. (G) Heatmap of scaled transcript expression of neuronal differentiation markers in control or SMARCB1 knockdown neurons differentiated with Day 0 doxycycline. VIM, HES1, HES5, PAX6, and EOMES are markers of less differentiated neural cells. All other genes are markers of committed neurons.

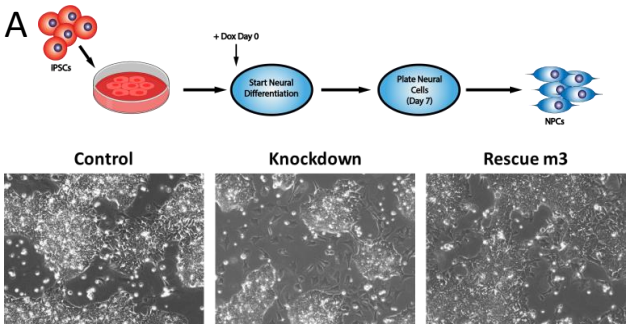
A
iPSCs
+ Dox Day 0
Start Neural Differentiation
Plate Neural Cells (Day 7)
NPCs
Control
Knockdown
Rescue m3

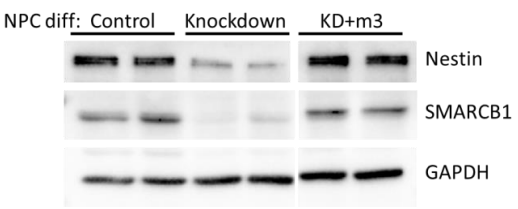
B
NPC diff: Control
Knockdown
KD+m3
Nestin
SMARCB1
GAPDH

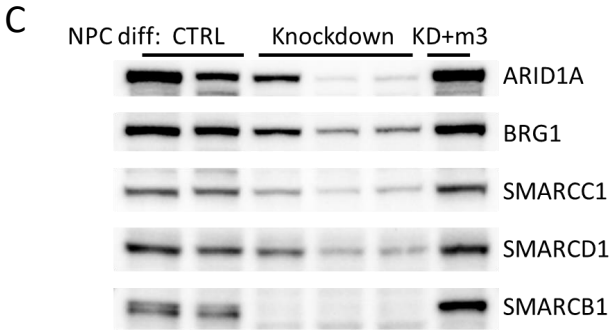
C
NPC diff: CTRL
Knockdown
KD+m3
ARID1A
BRG1
SMARCC1
SMARCD1
SMARCB1

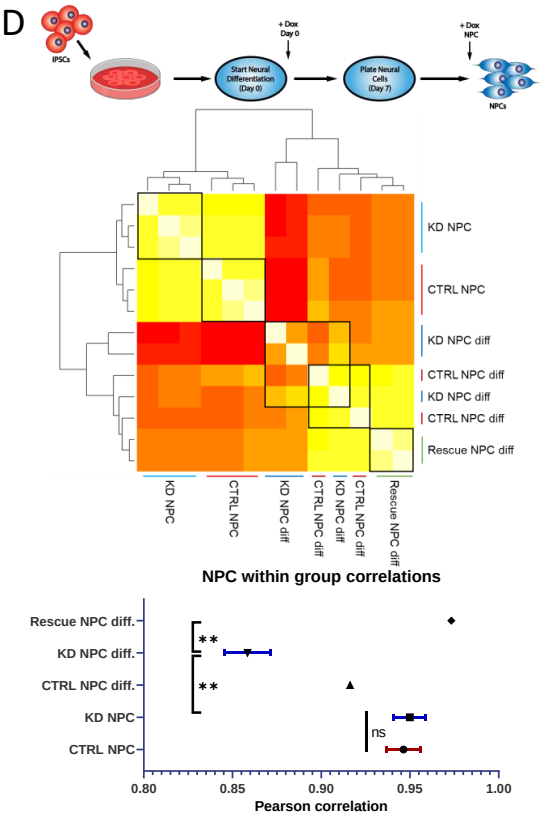
D
iPSCs
+ Dox Day 0
Start Neural Differentiation (Day 0)
Plate Neural Cells (Day 7)
+ Dox NPC
NPCs
KD NPC
CTRL NPC
KD NPC diff
CTRL NPC diff
KD NPC diff
CTRL NPC diff
Rescue NPC diff
NPC within group correlations
Rescue NPC diff.
KD NPC diff.
CTRL NPC diff.
KD NPC
CTRL NPC
**
**
ns
0.80
0.85
0.90
0.95
1.00
Pearson correlation

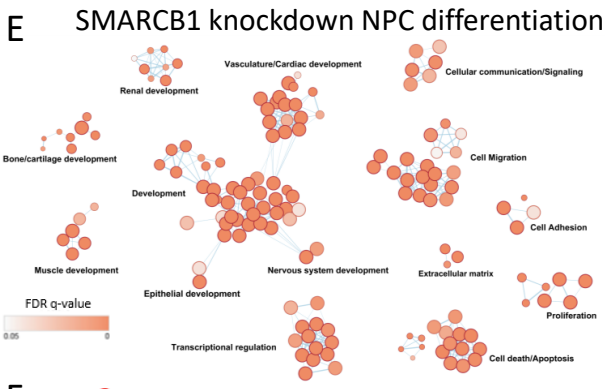
E
SMARCB1 knockdown NPC differentiation
Renal development
Vasculature/Cardiac development
Cellular communication/Signaling
Bone/cartilage development
Development
Cell Migration
Cell Adhesion
Muscle development
Nervous system development
Extracellular matrix
Epithelial development
Proliferation
Transcriptional regulation
Cell death/Apoptosis
FDR q-value

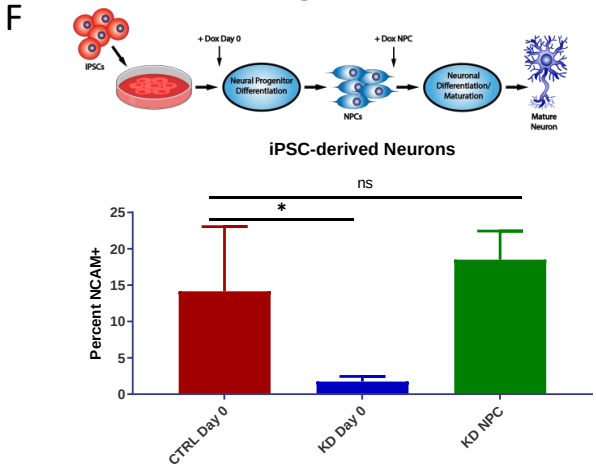
F
iPSCs
+ Dox Day 0
Neural Progenitor Differentiation
+ Dox NPC
NPCs
Neuronal Differentiation/ Maturation
Mature Neuron
iPSC-derived Neurons
ns
*
Percent NCAM+
25
20
15
10
5
0
CTRL Day 0
KD Day 0
KD NPC

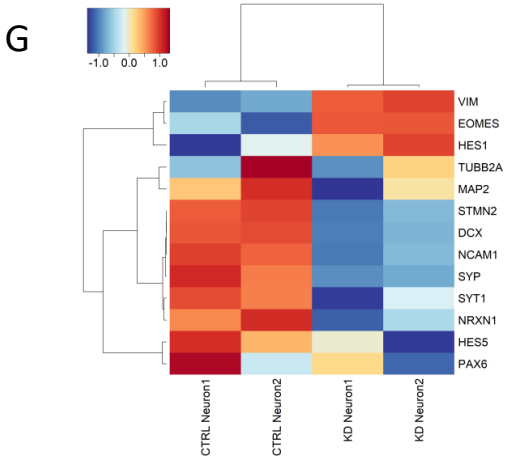
G
-1.0
0.0
1.0
VIM
EOMES
HES1
TUBB2A
MAP2
STMN2
DCX
NCAM1
SYP
SYT1
NRXN1
HES5
PAX6
CTRL Neuron1
CTRL Neuron2
KD Neuron1
KD Neuron2

To validate results from the organoid model and further assess the interaction between SMARCB1 loss and differentiation, control and knockdown cells were subjected to in vitro directed neuronal differentiation (50). Neuronal maturation efficacy was measured using FACS analysis for surface expression of NCAM, a marker of mature neurons. Cells subjected to SMARCB1 knockdown during both NPC and neuronal differentiation had lower numbers of NCAM positive cells after 25 days of neuronal differentiation and maturation than control cells, as well as when compared to cells subjected to knockdown beginning at the NPC state (Figure 4.1F). RNA-seq analysis of control and knockdown neurons showed a reduction in the expression of neuronal markers in cells differentiated in the absence of SMARCB1, along with a retention of some markers of earlier stages of neural differentiation (Figure 4.1G) This suggests that SMARCB1 loss during neuronal differentiation leads to a failure in maturation in multiple contexts and validates that cells are particularly vulnerable to SMARCB1 loss early in neural development. This window of vulnerability is consistent between organoid and directed neuronal differentiation experiments, and demonstrates a similar trend to that previously observed in an inducible SMARCB1 knockout mouse model (11).

Figure 4.2. NPCs differentiated without SMARCB1 are prone to changes in morphology and may demonstrate enhanced proliferation or dependency on continued SMARCB1 loss. (A) ATPlite growth curve of one differentiation batch of control, rescue and SMARCB1 knockdown NPCs differentiated with doxycycline (Day 0) compared to induction with doxycycline post-differentiation (NPC). * indicates a p-value < 0.05, *** indicates a p-value < 0.001. This phenotype was not observed in all batches of differentiation but illustrates a flexibility in NPCs differentiated without SMARCB1 to display unusual changes in morphology or phenotype. (B) Diagram comparing genes differentially expressed in SMARCB1 knockdown condition relative to control in NPCs differentiated without SMARCB1 (NPC diff.) and NPCs induced with doxycycline post-differentiation (NPC). (C) Gene ontology network of genes unique to SMARCB1 knockdown at the NPC state and not altered in NPCs differentiated without SMARCB1. Dots represent statistically significant gene ontology terms, clustered based on overlap of the genes contained in each term. Dot size indicates the number of genes included in each term and darker color corresponds to smaller adjusted p-value. Labels indicate the main process making up each cluster. (D) Above, schematic showing time-course experiment with doxycycline induction at various time points throughout the NPC differentiation process. Below, qRT-PCR analysis showing transcript levels and standard deviation relative to control mean for SMARCB1 and neural progenitor markers Pax6 and Nestin. Upper bars indicate most conservative significance levels between control and knockdown. Lower bars indicate significance between knockdown timepoints. Comparisons were conducted using two-way ANOVA with Tukey's multiple comparisons test. * indicates adjusted p-value < 0.05, ** indicates adjusted p-value < 0.01, *** indicates adjusted p-value < 0.001.

A

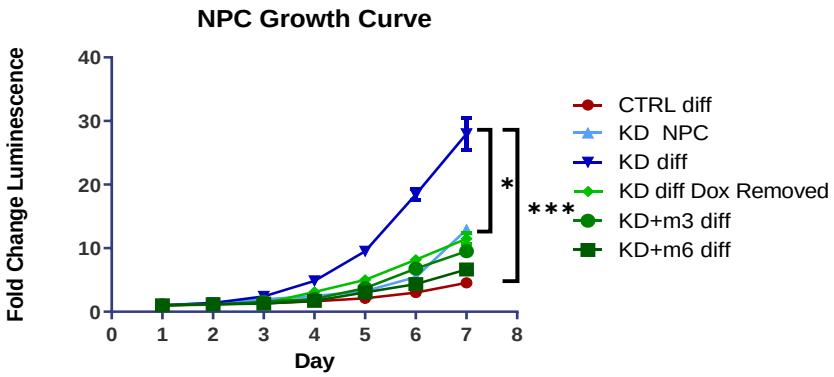
NPC Growth Curve
Fold Change Luminescence
Day
CTRL diff
KD NPC
KD diff
KD diff Dox Removed
KD+m3 diff
KD+m6 diff
*
***

B

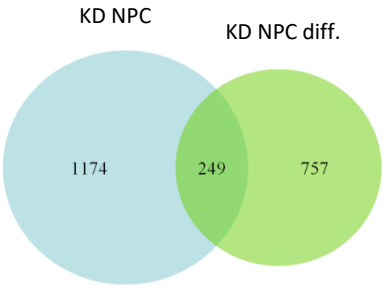
KD NPC
KD NPC diff.
1174
249
757

C

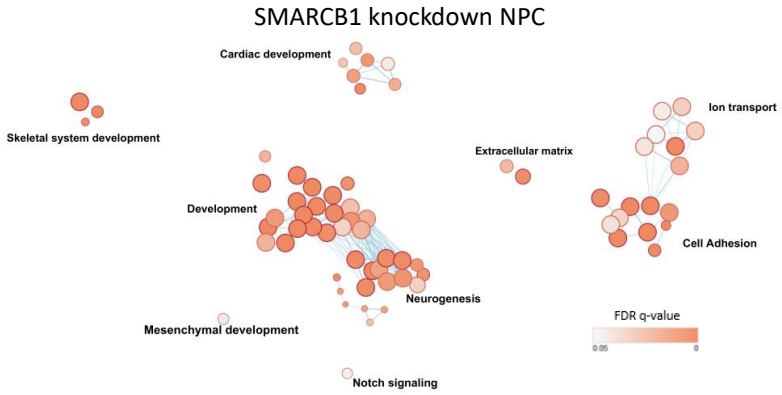
SMARCB1 knockdown NPC
Cardiac development
Skeletal system development
Development
Neurogenesis
Mesenchymal development
Notch signaling
Extracellular matrix
Ion transport
Cell Adhesion
FDR q-value

D

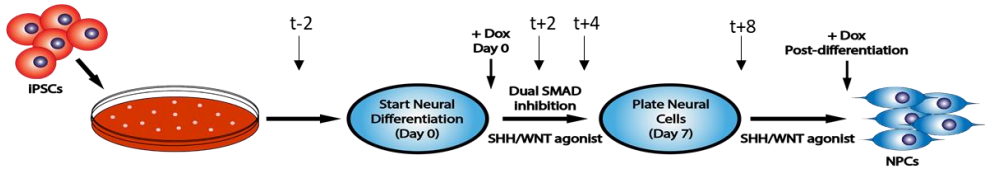
IPSCs
t-2
+ Dox
Day 0
t+2
t+4
t+8
+ Dox
Post-differentiation
Start Neural Differentiation (Day 0)
Dual SMAD Inhibition
SHH/WNT agonist
Plate Neural Cells (Day 7)
SHH/WNT agonist
NPCs

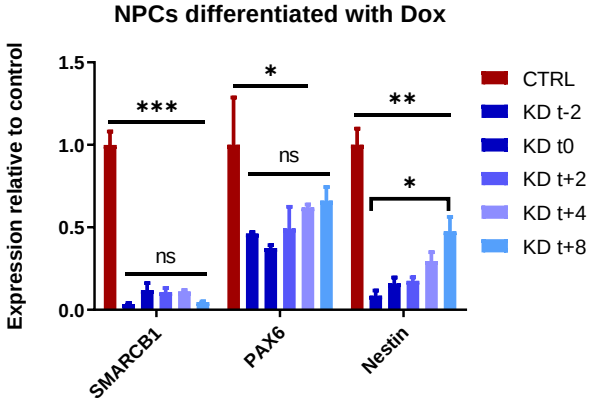
NPCs differentiated with Dox
Expression relative to control
CTRL
KD t-2
KD t0
KD t+2
KD t+4
KD t+8
***
ns
*
ns
**
*
SMARCB1
PAX6
Nestin

4.3 Neural progenitors differentiated without SMARCB1 are transcriptionally similar to ATRT, particularly the SHH subgroup

It seems probable that these observed interactions between SMARCB1 loss and neural differentiation could play a role in ATRT tumorigenesis. To investigate this, previously published bulk RNA-seq data generated from ATRT tumors (14) was obtained in order to determine the similarity of this cellular model to patient tumors and to identify cell types with the greatest similarity. To compare the tumor data to the organoid scRNA-seq data, averaged transcriptomic data for each organoid cluster was computed and correlated to the ATRT samples (Figure 4.3A, S4.1A). While correlations were generally higher within the organoid or tumor groups, there was variability in the similarity of different organoid cell types to tumors. Neurons in the control organoids were the least similar to the tumors, while progenitor clusters in the SMARCB1 knockdown organoids were most similar (Figure 4.3A). This is consistent with the concept of a SMARCB1-deficient early neural progenitor acting as the cell of origin for ATRT. Progenitor clusters in the control organoids were generally less similar to the tumor samples than the same clusters in the knockdown organoids, with the least differentiated clusters (10, 12) showing the greatest similarity to tumors (Figure 4.3A). These clusters also demonstrate a possible (but not statistically significant with n=3 organoids) expansion in knockdown organoids relative to controls (Figure S3.2D), and thus their development may be favored in the absence of SMARCB1 expression. SMARCB1 knockdown progenitors also show changes in genes associated with transcriptional regulation, nervous system development, and extracellular matrix organization (Figure 3.4F), all pathways identified as being altered in ATRT (13, 14). Comparison of ATRT transcriptomes with RNA-seq data from control and SMARCB1 knockdown iPSCs and NPCs (Figure 4.3B-C) revealed greater ATRT similarity to NPCs differentiated without SMARCB1 than either knockdown iPSCs or NPCs induced with SMARCB1 loss post-differentiation. Previous transcriptomic and epigenomic analyses have identified three subgroups within ATRT with

differing epigenetic landscapes and gene expression profiles (13, 58). A comparison of both NPCs differentiated without SMARCB1 via small molecule-directed differentiation and progenitors within SMARCB1 knockdown organoids with ATRTs from each of the three subgroups revealed the greatest similarity with the SHH, or Neurogenic subgroup (Figure 4.3D, Figure S4.1A-C). This suggests a possible mechanism of ATRT tumorigenesis, likely most relevant to the SHH subgroup, in which focal deletion of SMARCB1 occurs early in neural development, leading to unstable NPCs with tendencies toward differentiation defects, cellular transformation and tumorigenesis.

Figure 4.3. Neural progenitor cells differentiated without SMARCB1 are transcriptomically similar to atypical teratoid rhabdoid tumors. (A) RNA sequencing data from 25 ATRTs (Johann et al. 2014) was compared to averaged single-cell RNA sequencing data for each cluster in control and SMARCB1 knockdown cerebral organoids. Left, chart of pearson correlation values between individual clusters and ATRT samples, clustered by similarity. White indicates highest correlation and red corresponds to lowest correlation. Labels indicate cell types corresponding to clusters. Box indicates region of highest similarity to ATRT samples. Upper right, schematic of protocol used for organoid generation. Lower right, mean and standard error of pearson correlation values of progenitors and neurons from control and SMARCB1 knockdown organoids. Comparisons between groups conducted using one-way ANOVA with Tukey's multiple comparisons test. *** indicates adjusted p-value < 0.001. (B) Top, schematic of protocol used for NPC differentiation either in the presence of doxycycline from Day 0 (NPCdiff) or at the NPC state (NPC). Bottom, principal component analysis of RNA sequencing results from 25 ATRT samples compared to directed differentiation of control or SMARCB1 knockdown iPSC-derived NPCs, along with BT16 ATRT cell line and undifferentiated iPSCs induced with doxycycline. (C) Top, chart of pearson correlation values between control and SMARCB1 knockdown iPSCs and NPCs, induced with doxycycline during and post-differentiation, along with ATRT samples, clustered by similarity. White indicates highest correlation and red corresponds to lowest correlation. Box indicates region of highest similarity to ATRT samples. Bottom, mean and standard error of pearson correlation values of control and SMARCB1 knockdown NPCs and BT16 cell line with ATRT samples. Comparisons between groups conducted using one-way ANOVA with Tukey's multiple comparisons test. * indicates adjusted p-value < 0.05 and *** indicates adjusted p-value < 0.001. (D) Mean and standard error of pearson correlation values of NPCs differentiated without SMARCB1 and samples from each of the three ATRT subgroups. Comparisons between groups conducted using one-way ANOVA with Tukey's multiple comparisons test. ** indicates adjusted p-value < 0.01.

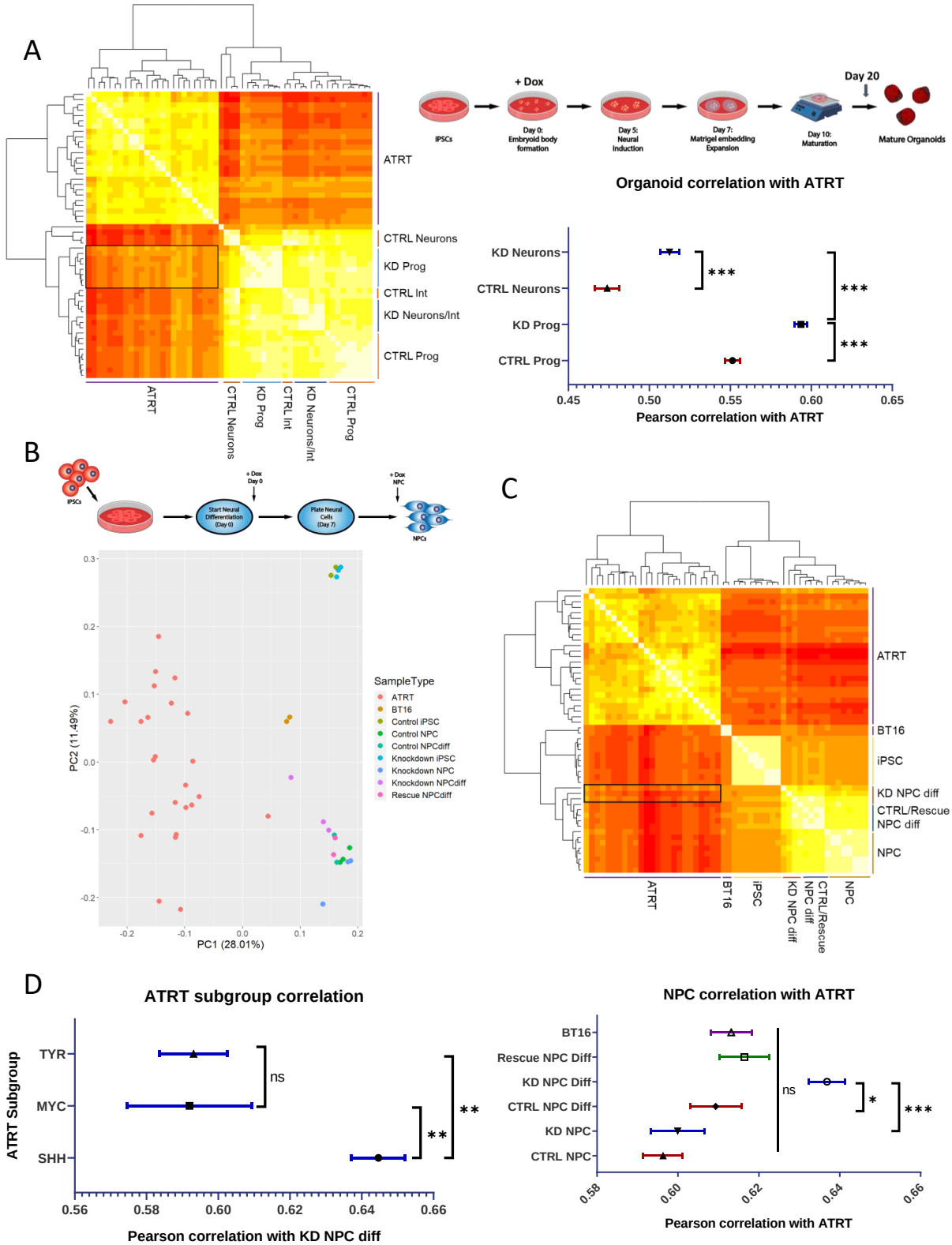
A
ATRT
CTRL Neurons
KD Prog
CTRL Int
KD Neurons/Int
CTRL Prog
+ Dox
Day 20
IPSCs
Day 0: Embryoid body formation
Day 5: Neural Induction
Day 7: Matrigel embedding Expansion
Day 10: Maturation
Mature Organoids
Organoid correlation with ATRT
KD Neurons
CTRL Neurons
KD Prog
CTRL Prog
***
***
***
0.45
0.50
0.55
0.60
0.65
Pearson correlation with ATRT
B
iPSCs
Start Neural Differentiation (Day 0)
Plate Neural Cells (Day 7)
NPCs
+ Dox Day 0
+ Dox NPC
PC2 (11.49%)
PC1 (28.01%)
SampleType
ATRT
BT16
Control iPSC
Control NPC
Control NPCdiff
Knockdown iPSC
Knockdown NPC
Knockdown NPCdiff
Rescue NPCdiff
C
ATRT
BT16
iPSC
KD NPC diff
CTRL/Rescue NPC diff
NPC
D
ATRT subgroup correlation
ATRT Subgroup
TYR
MYC
SHH
ns
**
**
0.56
0.58
0.60
0.62
0.64
0.66
Pearson correlation with KD NPC diff
NPC correlation with ATRT
BT16
Rescue NPC Diff
KD NPC Diff
CTRL NPC Diff
KD NPC
CTRL NPC
ns
*
***
0.58
0.60
0.62
0.64
0.66
Pearson correlation with ATRT

4.4 Neural progenitor cells differentiated without SMARCB1, but not NPCs induced with SMARCB1 loss post-differentiation, are capable of xenograft formation in mice

To test the ability of SMARCB1-deficient neural progenitors to initiate tumorigenesis, shControl and shSMARCB1 NPCs differentiated without doxycycline induction were induced at the NPC stage to initiate SMARCB1 loss and injected into mouse cerebellums (Figure 4.4A). Mice were monitored for weight loss or neurological symptoms indicative of cerebellar tumor formation. When these NPCs differentiated with intact SMARCB1 expression were injected, both control and SMARCB1 knockdown NPCs failed to form tumors. Six to eight months post-injection, mice injected with both control and knockdown NPCs began to demonstrate weight loss and the experiment was concluded, although formation of large intracranial tumors near the injection site was not visible (Figure 4.4A). There were no statistically significant differences in the survival of mice injected with control and knockdown NPCs (Figure 4.4A). However, when NPCs differentiated without SMARCB1 were injected into mice, visible tumors formed over the course of three to six months in all mice injected (Figure 4.4B). Absence of doxycycline treatment to the mice was sufficient to prevent tumor formation. Human nuclei staining revealed that SMARCB1-deficient cells were able to continue to proliferate within the mice, forming visible tumors near the injection site and leading to a statistically significant reduction of survival compared to mice not treated with doxycycline (Figure 4.4B).

This data further supports the concept of an interaction between SMARCB1 loss and neural differentiation state. It seems that cells early in the neural differentiation process are sensitized towards tumorigenesis resulting from SMARCB1 loss, while undifferentiated cells are unable to tolerate the loss and committed neural progenitors are resistant to transformative effects. These observations are consistent with the early age of onset of rhabdoid tumors, restricted tissues of origin and rarity of SMARCB1 loss of function mutations in other tumor types.

Figure 4.4. Neural progenitor cells differentiated without SMARCB1, but not NPCs with post-differentiation knockdown, are capable of forming tumors orthotopically in mice. A) Left, survival curves of mice injected with control or SMARCB1 knockdown NPCs induced with doxycycline at the NPC state. Right, human nuclei staining of a sample shSMARCB1 NPC cerebellum near the injection site. B) Left, survival curves of mice injected with NPCs differentiated without SMARCB1, either with doxycycline removed or in the continued presence of doxycycline. Statistical comparisons were conducted using the log-rank (Mantel-Cox) test. ** indicates a p-value < 0.01. Right, human nuclei staining of a sample mouse cerebellum injected with shSMARCB1 NPCdiff and maintained with dox.

A

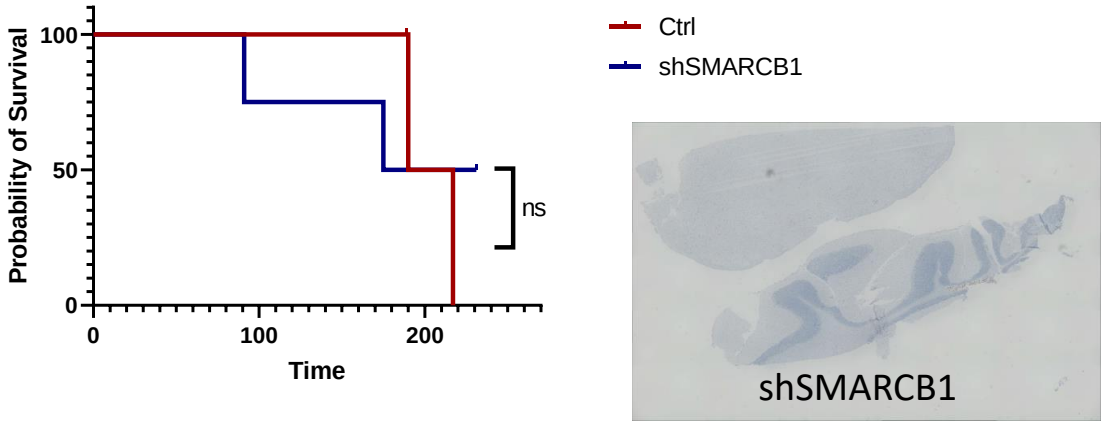
NPCs induced post-differentiation
Probability of Survival
100
50
0
0
100
200
Time
ns
Ctrl
shSMARCB1
shSMARCB1

B

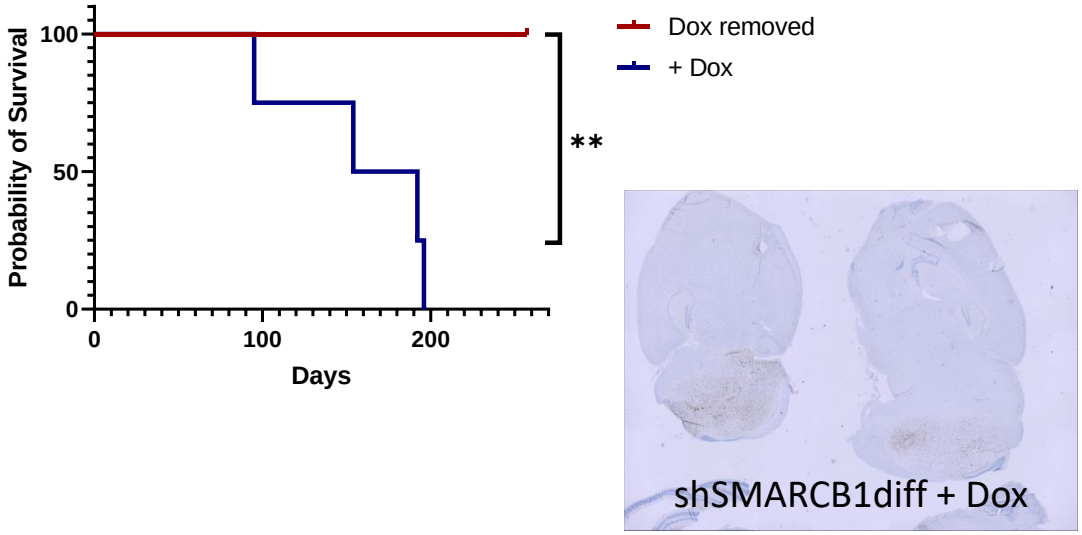
NPCs differentiated without SMARCB1
Probability of Survival
100
50
0
0
100
200
Days
**
Dox removed
+ Dox
shSMARCB1diff + Dox

4.5 Perspectives and conclusions

SMARCB1 is an important chromatin remodeling subunit as well as a known tumor suppressor whose loss is the primary driver of pediatric rhabdoid tumors. In this study we have interrogated the interactions between SMARCB1 loss, cellular differentiation state, and transcriptional changes associated with tumorigenesis, while generating a cellular model which will have utility for future mechanistic studies as well as for identification of potential therapeutic vulnerabilities in SMARCB1-deficient cells. While other systems of SMARCB1 loss or reintroduction have been used to study the mechanisms underlying ATRT in a controlled manner (11, 12, 24, 25, 38, 59), this complementary system has the benefit of using human cells, having the flexibility to take into account the effects of differentiation processes, and using SMARCB1 loss alone without additional oncogenic drivers, consistent with the human tumor phenotype (8). In addition, similar to a recent publication (59), our study provides an interrogation of the interactions between SMARCB1 loss and neural development, however, here we illustrate novel insight into the dramatic phenotypic differences which can occur with loss of SMARCB1 at different stages of differentiation, such as lethality in pluripotent cells and impairment of neuronal commitment and maturation. This is the first study to model the interaction between SMARCB1 loss and cellular differentiation state that likely contributes to ATRT tumorigenesis in human cells, and to monitor the accompanying gene expression and phenotypic changes.

We have demonstrated significant differences in the response of cells to SMARCB1 loss at differing stages of neural differentiation and identified a window early in neural commitment in which cells seem to be particularly vulnerable to SMARCB1 loss of function and in which SMARCB1 loss results in profound defects in the progression of differentiation. SMARCB1 loss during this period results in cells with greater similarity to ATRT tumors than loss at an earlier pluripotent or later committed neural progenitor state, along with a lack of stability resulting in a tendency toward stochastic alterations in cellular morphology and gene expression. This provides insight into a possible mechanism for ATRT tumorigenesis in which a loss of SMARCB1

during embryogenesis could result in cells which are primed for cellular transformation. This is consistent with both the early age of onset of this disease and heterogeneity of presentation, as well as with mouse data showing development of ATRT-like tumors with SMARCB1 loss during early mouse embryogenesis (11). While it is clear that the neural progenitors differentiated without SMARCB1 in this study are most similar to the SHH/Neurogenic subgroup of ATRT, more work is needed to determine the mechanism underlying this similarity. It is possible that the transcriptomic and epigenetic differences between the subgroups are driven by different cells or developmental stages of origin, and the origin of SHH/Neurogenic tumors more closely resembles the loss of function early in development which was applied in this study. Indeed, the SHH/Neurogenic subgroup of tumors does tend to occur in younger children, consistent with this hypothesis (13, 14). Another possibility is that the mechanism of SMARCB1 loss could play a role, with the larger chromosomal alterations observed more often in the other subgroups of ATRT leading to additional effects on neighboring genes or regulatory regions not replicated with a knockdown model. Thus, the predominance of smaller focal or point mutations in the SHH subgroup might more closely resemble a SMARCB1 knockdown system.

In this study we focused on the interactions of SMARCB1 loss with neural development, but molecular heterogeneity and dysregulated developmental pathways observed in extra-cranial malignant rhabdoid tumors (15, 60) suggest that a similar mechanism might take place in other types of rhabdoid tumors. In all, we have presented an in depth investigation into the stages of neural differentiation in which SMARCB1 loss has the greatest effects on cellular outcome, chronicled gene expression changes resulting from SMARCB1 loss at various stages of differentiation and generated a novel platform on which to expand our understanding on the mechanisms and vulnerabilities underlying ATRT tumorigenesis.

4.6 Methods

4.6.1 Pluripotent stem cell culture and neural differentiations

iPSCs were induced to form neural progenitor cells using a small-molecule based differentiation protocol as described in Reinhardt et al. (50), using combined small-molecule inhibition of BMP and TGF β signaling along with WNT and SHH pathway stimulation. Neuron differentiations were also conducted as described in Reinhardt et al. for peripheral neurons (50), starting from NPCs of 3-6 passages in smNPC maintenance medium (N2B27 medium + CHIR + PMA). Neurons were harvested after two weeks in neuronal maturation medium (N2B27 medium + dbcAMP + TGF-b3 + BDNF + GDNF). Both neural progenitor and neuron differentiations were conducted under 0.5 μg/mL puromycin to prevent loss of shRNA expression. Rescue cell lines were differentiated in the presence of 0.5 μg/mL puromycin and 100 μg/mL G418. When needed, doxycycline was applied at a 1 μg/mL concentration for all experiments.

4.6.2 Western blots and immunoprecipitations

For western blots, cells were lysed in RIPA lysis buffer with proteinase and phosphatase inhibitors. 20 μg lysate was run on an SDS-PAGE gel, transferred at 350 mA over 1.5 hours to EMD Millipore Immobilon-P PVDF membrane, blocked for one hour in 5% BSA, and probed with primary antibody overnight. Membranes were washed with PBS + 0.1% Tween-20, probed for 1-2 hours with secondary HRP-conjugated antibody and exposed using Thermo Scientific SuperSignal West Pico or Femto Chemiluminescent Substrate. For BAF complex immunoprecipitations, nuclear extractions were first performed using Thermo Scientific NE-PER Nuclear and Cytoplasmic Extraction Reagents (78833) according to kit instructions. For immunoprecipitations, 2 μg of BRG1 antibody (Santa Cruz, sc-17796) was incubated for one hour with 20 μL Dynabeads Protein G magnetic beads (Thermo Fisher Scientific, 10004D), washed, then incubated overnight at 4 C with 500 μg of nuclear lysate, washed and prepared for SDS-PAGE. Washes were conducted with either citric or RIPA buffer, as specified. Western blots were run

as previously described. Primary antibodies used for western blots were: SMARCB1/BAF47 (mouse, 1:500, BD Biosciences, 612110), GAPDH (rabbit, 1:5000, 2118), HDAC1 (rabbit, 1:1000, Cell Signaling, 2062), SMARCD1 (mouse, 1:1000, Santa Cruz, sc-135843), SMARCC1 (rabbit, 1:1000, Santa Cruz, sc-10756), BRG1 (mouse, 1:1000, Santa Cruz, sc-17796), Nestin (rabbit, 1:1000, EMD Millipore).

4.6.3 Bulk RNA sequencing preparation and analysis

RNA was extracted using Qiagen RNeasy Plus Mini Kit and library prep was conducted using Illumina NEBNext Ultra Directional Library Prep Kit. Samples were sequenced using an Illumina sequencer with a minimum of 20 million reads per sample. Transcriptome data was aligned using the STAR aligner to a reference human genome (hg19). Reads were counted using featureCounts with default settings, and differential expression analysis conducted using DESeq2 R package (61). Significant genes were considered to be those with a Benjamini-Hochberg adjusted p-value of greater than 0.05 and a fold-change of greater than 2. Gene ontology analysis for upregulated and downregulated genes was conducted using the GOrilla web-based tool (56), comparing a list of up to 500 most significant genes (based on adjusted p-value) to a background list of all expressed genes (rpkm $>$ 4 across all samples). For gene ontology networks, top 500 significant genes were analyzed for GO biological process and Reactome biological pathway enrichment by gProfiler (62) and output file visualized using Cytoscape (63) software with EnrichmentMap plugin (64).

4.6.4 Flow cytometry

For neuron FACS experiments, Day 25 neurons were dissociated with Accutase + DNase I for 30 minutes, with occasional gentle pipetting to break up clumps. Cells were filtered through a cell strainer and resuspended in PBS + 1% FBS. 1×10^6 cells were stained with NCAM-1 antibody (CD56 Anti human Alexafluor 700, 1:200 dilution, Fisher Scientific, BDB557919) for 1 hour, washed three times with PBS + 1% FBS, and analyzed on a Sony SH800 instrument.

4.6.5 Mouse xenograft experiments

Animal research experiments were approved by the UCSD Animal Care Program, protocol number S00192M. Control and SMARCB1 knockdown NPCs induced with doxycycline for 7 days prior to injection were dissociated using accutase (Innovative Cell Technologies), washed with PBS, and resuspended at 1×10^6 cells in 2 μL PBS supplemented with 0.1% BSA per animal. Animals were fed doxycycline chow for a week prior to injections and for the duration of the experiment. Resuspended cells were kept on ice and were inoculated into the cerebellum of 4–6 week-old female Nod scid mice (Charles River Laboratory) by stereotactic injections (2.0 mm posterior and 2.0 mm to the right of the bregma, and 3 mm deep from the inner plate of the skull). Animals were sacrificed when weight loss was detected or animals began showing neurological symptoms.

4.7 Supplementary Figures

Figure S 4.1. NPCs differentiated with SMARCB1 knockdown are most similar to the SHH/Group 1 subtype of ATRT in both organoid and directed differentiation models. (A) RNA sequencing data from 25 ATRTs was compared to averaged single-cell RNA sequencing data for each cluster in control and SMARCB1 knockdown cerebral organoids. Left, chart of pearson correlation values between individual clusters and ATRT samples, clustered by similarity and labeled by subgroup designation (Johann et al. 2014). White indicates highest correlation and red corresponds to lowest correlation. Labels indicate cell types corresponding to clusters. Box indicates region of highest similarity between ATRT subgroup and organoid clusters. Right, mean and standard error of pearson correlation values of progenitors from SMARCB1 knockdown organoids with ATRTs from each subgroup. Comparisons between groups conducted using one-way ANOVA with Tukey's multiple comparisons test. *** indicates adjusted p-value < 0.001. ** indicates p-value < 0.01. (B) Principal component analysis of RNA sequencing results from 25 ATRT samples, labeled by corresponding subgroup where known, compared to directed differentiation of control or SMARCB1 knockdown iPSCs differentiated into NPCs in the presence of doxycycline (NPCdiff) or at the NPC state (NPC), along with BT16 ATRT cell line and undifferentiated iPSCs induced with doxycycline. (C) Chart of pearson correlation values between control and SMARCB1 knockdown iPSCs and NPCs, induced with doxycycline during and post-differentiation, along with ATRT samples, clustered by similarity and labeled by subgroup designation (Johann et al. 2014). White indicates highest correlation and red corresponds to lowest correlation. Box indicates region of highest similarity between ATRT subgroup and SMARCB1 knockdown model.

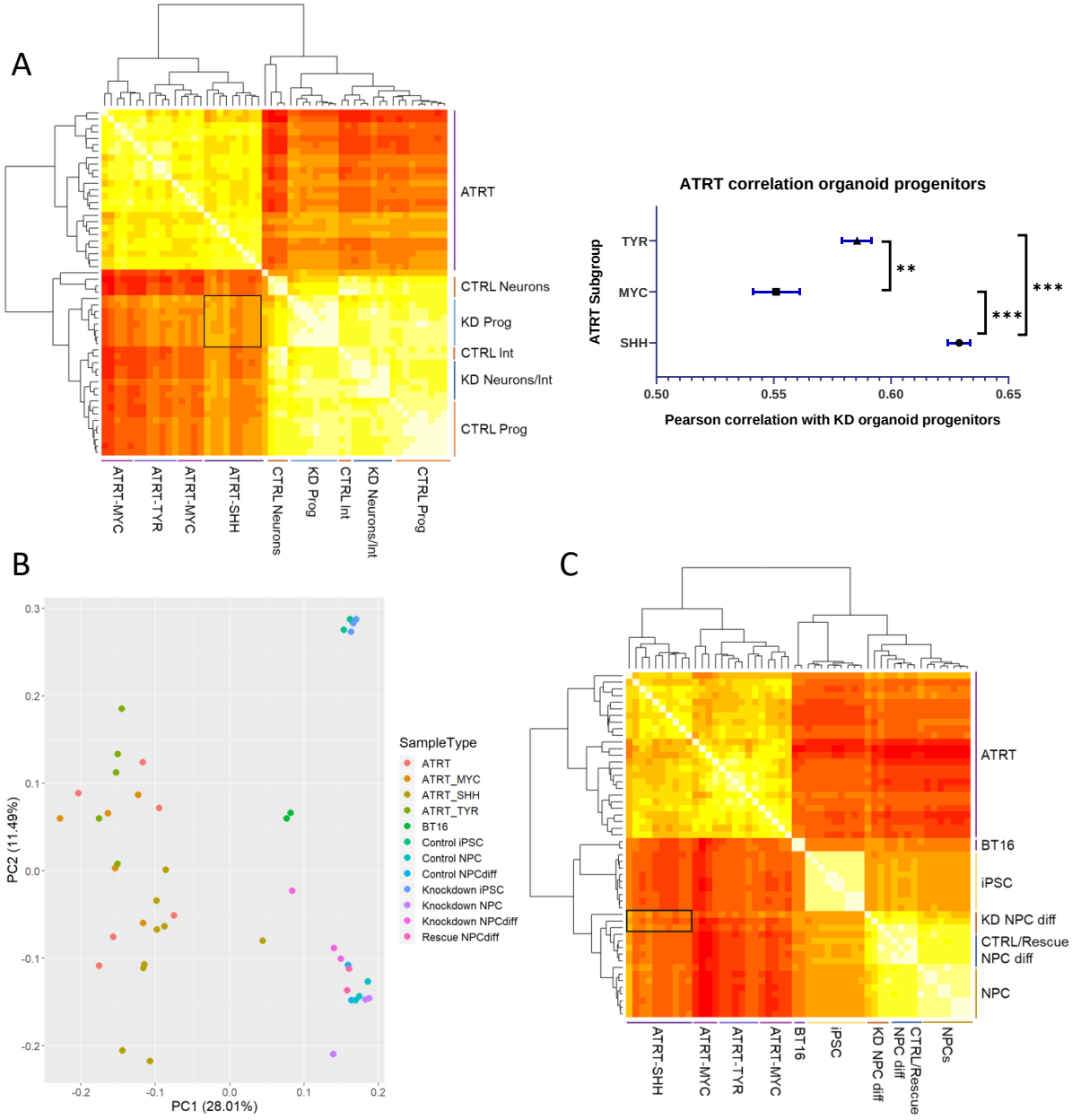
A
ATRT
CTRL Neurons
KD Prog
CTRL Int
KD Neurons/Int
CTRL Prog
ATRT-MYC
ATRT-TYR
ATRT-MYC
ATRT-SHH
CTRL Neurons
KD Prog
CTRL Int
KD Neurons/Int
CTRL Prog
ATRT correlation organoid progenitors
ATRT Subgroup
TYR
MYC
SHH
**
***
***
0.50
0.55
0.60
0.65
Pearson correlation with KD organoid progenitors
B
PC2 (11.49%)
PC1 (28.01%)
SampleType
ATRT
ATRT_MYC
ATRT_SHH
ATRT_TYR
BT16
Control iPSC
Control NPC
Control NPCdiff
Knockdown iPSC
Knockdown NPC
Knockdown NPCdiff
Rescue NPCdiff
C
ATRT
BT16
iPSC
KD NPC diff
CTRL/Rescue NPC diff
NPC
ATRT-SHH
ATRT-MYC
ATRT-TYR
ATRT-MYC
BT16
iPSC
KD NPC diff
CTRL/Rescue NPC diff
NPCs

4.8 Acknowledgements

Chapter 4 contains modified material as it appears in Parisian AD, Koga T, Miki S, Johann PD, Kool M, Crawford JR, Furnari FB (2020). ”SMARCB1 loss interacts with neuronal differentiation state to block maturation and impact cell stability.” Genes & Development. The dissertation author is the primary author of this paper.

I would like to thank Dr. Shunichiro Miki and Dr. Ciro Zanca for their assistance in mouse xenograft experiments for this project. I would also like to thank Drs. Pascal Johann and Marcel Kool for their contributions of ATRT RNA-seq data, which were invaluable to this manuscript.

This work was supported by Padres Pedal the Cause/RADY grant (PTC2017), the National Institute of General Medical Sciences T32GM008666 (A.P.), the National Institute of Neurological Diseases and Stroke R01-NS080939 (F.F.), and a Japan Society for the Promotion of Science (JSPS) Overseas Research Fellowship (S.M.).

Chapter 5

Conclusions and Future Directions

In summary, I have developed an inducible SMARCB1-deficient induced pluripotent stem cell line in order to model ATRT tumorigenesis and investigate interactions between SMARCB1 loss and neural differentiation state. While initial experiments inducing genetic knockout of SMARCB1 using CRISPR-Cas9 methodology ultimately failed to generate homozygous knockout clones, these experiments gave us early insight into the ability of SMARCB1 loss to initiate cell death in certain developmental contexts. In addition, an inducible system provides versatility, allowing initiation of knockdown at various timepoints throughout a differentiation process or in differentiated cells. These studies have demonstrated the utility and flexibility of an engineered pluripotent cell line to investigate roles of developmental processes in tumorigenesis. While we specifically used this system to look at the interactions between SMARCB1 loss and neural differentiation, it would be possible to apply this cell line to other developmental contexts as well. Future applications could include studying the developmental context of kidney rhabdoid tumor tumorigenesis or identifying whether differentiation down alternate lineages can lead to the formation of cells resembling Group 2A/TYR or Group 2B/MYC ATRT. This cell line also has an important potential application for in vitro drug screening to identify putative ATRT therapeutics. NPCs differentiated without SMARCB1 represent an ideal candidate for use in drug screens due to their demonstrated transcriptional similarity to ATRT, proliferative and tumorigenic capacity, and the presence of a relevant isogenic control in the shControl cell

line or shSMARCB1 line in the absence of doxycycline induction. These properties will allow for ease of identifying drugs with a deleterious effect on growth of SMARCB1-deficient cells and removing those which also affect the proliferation or viability of wild-type cells. Given our data suggesting a role for blocked differentiation in ATRT tumorigenesis, screens could also be used to detect therapeutics capable of reversing this block and promoting cellular differentiation. Our results suggest that promoting tumor differentiation might block the progression of ATRT and could be a viable therapeutic strategy for these tumors. In addition, beyond developing a model for a single tumor type, the techniques we utilized to develop an in vitro model of ATRT could be replicated for many other conditions which involve a dysregulation of developmental processes in disease pathogenesis.

I applied this inducible SMARCB1 knockdown cell line to demonstrate differences in the phenotypic and transcriptional effects of SMARCB1 loss depending on cellular differentiation state. I determined that SMARCB1 loss in pluripotent cells is lethal, leading to decreased growth rate, loss of cellular adhesion and increased cell death. Additional studies could be performed investigating the mechanisms by which SMARCB1 loss leads to cell death in this context and which epigenetic or signaling patterns are required for SMARCB1 loss to have this effect. I additionally determined that, in contrast to pluripotent cells, SMARCB1 loss in committed neural progenitors leads to no obvious phenotypic effects, although detectable transcriptional changes do occur. These studies demonstrate the profound differences which can occur in the effect of an epigenetic regulator like SMARCB1 depending on cellular context and differentiation state. While it seems likely that the differences observed in transcriptional profiles due to SMARCB1 loss in different developmental contexts might be driven by differences in the epigenetic landscape, additional data is needed to determine this conclusively. Further studies will use chromatin immunoprecipitation sequencing (ChIP-seq) of histone marks and BAF complex binding to investigate the relationships between cellular epigenetic landscape, BAF complex activity and SMARCB1 loss.

Application of SMARCB1 knockdown during the process of neural development revealed

that the absence of SMARCB1 contributes to differentiation defects in a cerebral organoid model of neural development as well as during directed in vitro neuronal differentiation. In both of these differentiation systems, SMARCB1-deficient cells were not able to appropriately develop into mature neurons. In the organoid system, SMARCB1 knockdown organoids displayed a substantial reduction in the number of mature neurons which formed, while in the directed neuronal differentiation system, neural progenitors differentiated without SMARCB1 were deficient in their ability to express markers of mature neurons after a 25 day neuronal differentiation and maturation protocol. This data illustrates that SMARCB1 plays an important role in the process of neural differentiation, particularly the commitment and maturation of neurons. While this is an interesting observation, the mechanisms underlying this effect are yet to be determined. Future studies could investigate whether these effects of SMARCB1 loss on neural differentiation capacity are unique to SMARCB1 or whether other means of reducing BAF complex activity might have similar effects. It also remains to be determined whether SMARCB1 is uniquely involved in neuronal differentiation, or whether other cell lineages are similarly affected by SMARCB1 loss.

In addition to impaired neural differentiation, cells subjected to SMARCB1 loss throughout the neural developmental process displayed a marked loss of cellular stability. These cells displayed higher morphological and transcriptional variability, particularly over multiple passages, compared to control or SMARCB1 rescue cells. While control and rescue cells could be maintained at the NPC state for many passages without noticeable phenotypic changes, NPCs differentiated without SMARCB1 were prone to spontaneous changes in cellular morphology and growth rate, accompanied by transcriptional alterations. These cells were shown to be capable of cerebellar xenograft formation in mice, and to be more tumorigenic than both control NPCs and SMARCB1 knockdown NPCs which were induced with doxycycline at the NPC state. In addition, transcriptional profiles of these cells showed the greatest similarity to ATRT transcriptomes of all cell types analyzed. This combination of findings leads to a hypothesis of ATRT tumorigenesis where early neural progenitors with SMARCB1 mutations are unable to

differentiate normally, become trapped in a progenitor state, and are prone to transcriptional (and possibly epigenetic) alterations which lead to tumorigenesis (Figure 5.1). Additional studies analyzing the epigenetic landscapes of NPCs differentiated without SMARCB1 will elucidate whether this observed transcriptional and phenotypic instability is driven by an inability of SMARCB1-deficient cells to appropriately maintain a particular chromatin architecture.

In all, I have developed a novel cell-based model of atypical teratoid rhabdoid tumors which can be applied to future studies and therapeutic screens. I have identified contributions of the gene SMARCB1 to the process of neural development, and neuronal maturation in particular.

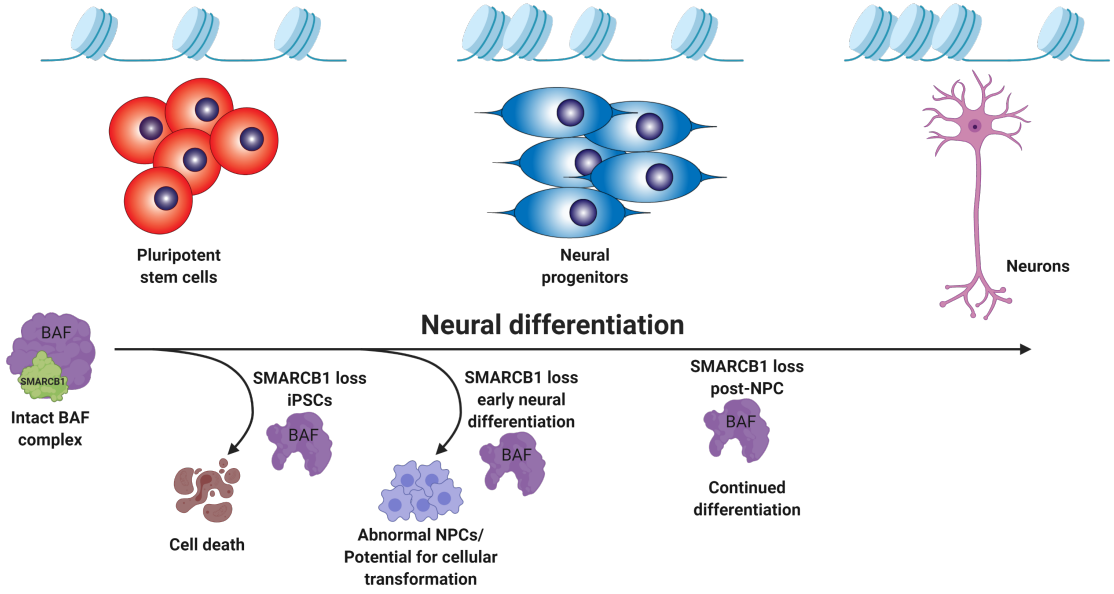

Figure 5.1. SMARCB1 loss interacts with developmental state to redirect cell fate. Schematic summarizing findings on the interaction between neural differentiation state and the effect of SMARCB1 loss. In pluripotent cells, SMARCB1 loss results in cell death. In the early stages of neural differentiation, SMARCB1 loss induces dedifferentiation, morphology changes and lack of stability in resulting NPCs along with defects in capacity for further neuronal differentiation. With induction of knockdown in later stages of differentiation, little to no effect on differentiation capacity or cell growth was observed.

And I have observed alterations in cellular stability driven by interactions between SMARCB1 loss and the process of neural differentiation which may contribute to cellular transformation and tumorigenesis. While many questions regarding the role of SMARCB1 in development and mechanisms of ATRT tumorigenesis remain unanswered, in this work I have provided substantial contributions to the field of ATRT research and developed a model system which can be applied to many future studies.

References

1. K. F. Ginn, A. Gajjar, Atypical teratoid rhabdoid tumor: current therapy and future directions. Frontiers in oncology 2, 114 (2012).

2. C. W. M. Roberts, S. H. Orkin, The SWI/SNF complex–chromatin and cancer. Nature reviews. Cancer 4, 133-142 (2004).

3. S. Venneti, P. Le, D. Martinez, S. X. Xie, L. M. Sullivan, L. B. Rorke-Adams, B. Pawel, A. R. Judkins, Malignant Rhabdoid Tumors Express Stem Cell Factors, Which Relate To the Expression of EZH2 and Id Proteins. The American Journal of Surgical Pathology 35, 1463-1472 (2011).

4. K. F. Ginn, A. Gajjar, Atypical teratoid rhabdoid tumor: current therapy and future directions. Front Oncol 2, 114 (2012).

5. I. Alimova, D. K. Birks, P. S. Harris, J. A. Knipstein, S. Venkataraman, V. E. Marquez, N. K. Foreman, R. Vibhakar, Inhibition of EZH2 suppresses self-renewal and induces radiation sensitivity in atypical rhabdoid teratoid tumor cells. Neuro Oncol 15, 149-160 (2013).

6. S. Venkataraman, I. Alimova, T. Tello, P. S. Harris, J. A. Knipstein, A. M. Donson, N. K. Foreman, A. K. Liu, R. Vibhakar, Targeting Aurora Kinase A enhances radiation sensitivity of atypical teratoid rhabdoid tumor cells. Journal of Neuro-Oncology 107, 517-526 (2012).

7. E. M. Jackson, A. J. Sievert, X. Gai, H. Hakonarson, A. R. Judkins, L. Tooke, J. C. Perin, H. Xie, T. H. Shaikh, J. A. Biegel, Genomic analysis using high-density single nucleotide polymorphism-based oligonucleotide arrays and multiplex ligation-dependent probe amplification provides a comprehensive analysis of INI1/SMARCB1 in malignant rhabdoid tumors. Clinical cancer research : an official journal of the American Association for Cancer Research 15, 1923-1930 (2009).

8. R. S. Lee, C. Stewart, S. L. Carter, L. Ambrogio, K. Cibulskis, C. Sougnez, M. S. Lawrence, D. Auclair, J. Mora, T. R. Golub, J. A. Biegel, G. Getz, C. W. M. Roberts, A remarkably simple genome underlies highly malignant pediatric rhabdoid cancers. The Journal of clinical investigation 122, 2983-2988 (2012).

9. B. S. Reincke, G. B. Rosson, B. W. Oswald, C. F. Wright, INI1 expression induces cell cycle arrest and markers of senescence in malignant rhabdoid tumor cells. Journal of cellular physiology 194, 303-313 (2003).

10. C. W. M. Roberts, M. M. Leroux, M. D. Fleming, S. H. Orkin, Highly penetrant, rapid tumorigenesis through conditional inversion of the tumor suppressor gene Snf5. Cancer Cell 2, 415-425 (2002).

11. Z. Y. Han, W. Richer, P. Freneaux, C. Chauvin, C. Lucchesi, D. Guillemot, C. Grison, D. Lequin, G. Pierron, J. Masliah-Planchon, A. Nicolas, D. Ranchere-Vince, P. Varlet, S. Puget, I. Janoueix-Lerosey, O. Ayrault, D. Surdez, O. Delattre, F. Bourdeaut, The occurrence of intracranial rhabdoid tumours in mice depends on temporal control of Smarcb1 inactivation. Nat Commun 7, 10421 (2016).

12. A. Carugo, R. Minelli, L. Sapio, M. Soeung, F. Carbone, F. S. Robinson, J. Tepper, Z. Chen, S. Lovisa, M. Svelto, S. Amin, S. Srinivasan, E. Del Poggetto, S. Loponte, F. Puca, P. Dey, G. G. Malouf, X. Su, L. Li, D. Lopez-Terrada, D. Rakheja, A. J. Lazar, G. J. Netto, P. Rao, A. Sgambato, A. Maitra, D. N. Tripathi, C. L. Walker, J. A. Karam, T. P. Heffernan, A. Viale, C. W. M. Roberts, P. Msaouel, N. M. Tannir, G. F. Draetta, G. Genovese, p53 Is a Master Regulator of Proteostasis in SMARCB1-Deficient Malignant Rhabdoid Tumors. Cancer Cell 35, 204-220.e209 (2019).

13. J. Torchia, B. Golbourn, S. Feng, K. C. Ho, P. Sin-Chan, A. Vasiljevic, J. D. Norman, P. Guilhamon, L. Garzia, N. R. Agamez, M. Lu, T. S. Chan, D. Picard, P. de Antonellis, D. A. Khuong-Quang, A. C. Planello, C. Zeller, D. Barsyte-Lovejoy, L. Lafay-Cousin, L. Letourneau, M. Bourgey, M. Yu, D. M. A. Gendoo, M. Dzamba, M. Barszczyk, T. Medina, A. N. Riemenschneider, A. S. Morrissy, Y. S. Ra, V. Ramaswamy, M. Remke, C. P. Dunham, S. Yip, H. K. Ng, J. Q. Lu, V. Mehta, S. Albrecht, J. Pimentel, J. A. Chan, G. R. Somers, C. C. Faria, L. Roque, M. Fouladi, L. M. Hoffman, A. S. Moore, Y. Wang, S. A. Choi, J. R. Hansford, D. Catchpoole, D. K. Birks, N. K. Foreman, D. Strother, A. Klekner, L. Bognar, M. Garami, P. Hauser, T. Hortobagyi, B. Wilson, J. Hukin, A. S. Carret, T. E. Van Meter, E. I. Hwang, A. Gajjar, S. H. Chiou, H. Nakamura, H. Toledano, I. Fried, D. Fults, T. Wataya, C. Fryer, D. D. Eisenstat, K. Scheinemann, A. J. Fleming, D. L. Johnston, J. Michaud, S. Zelcer, R. Hammond, S. Afzal, D. A. Ramsay, N. Sirachainan, S. Hongeng, N. Larbcharoensub, R. G. Grundy, R. R. Lulla, J. R. Fangusaro, H. Druker, U. Bartels, R. Grant, D. Malkin, C. J. McGlade, T. Nicolaides, T. Tihan, J. Phillips, J. Majewski, A. Montpetit, G. Bourque, G. D. Bader, A. T. Reddy, G. Y. Gillespie, M. Warmuth-Metz, S. Rutkowski, U. Tabori, M. Lupien, M. Brudno, U. Schuller, T. Pietsch, A. R. Judkins, C. E. Hawkins, E. Bouffet, S. K. Kim, P. B. Dirks, M. D. Taylor, A. Erdreich-Epstein, C. H. Arrowsmith, D. D. De Carvalho, J. T. Rutka, N. Jabado, A. Huang, Integrated (epi)-Genomic Analyses Identify Subgroup-Specific Therapeutic Targets in CNS Rhabdoid Tumors. Cancer Cell 30, 891-908 (2016).

14. P. D. Johann, S. Erkek, M. Zapatka, K. Kerl, I. Buchhalter, V. Hovestadt, D. T. Jones, D. Sturm, C. Hermann, M. Segura Wang, A. Korshunov, M. Rhyzova, S. Grobner, S. Brabetz,

L. Chavez, S. Bens, S. Groschel, F. Kratochwil, A. Wittmann, L. Sieber, C. Georg, S. Wolf, K. Beck, F. Oyen, D. Capper, P. van Sluis, R. Volckmann, J. Koster, R. Versteeg, A. von Deimling, T. Milde, O. Witt, A. E. Kulozik, M. Ebinger, T. Shalaby, M. Grotzer, D. Sumerauer, J. Zamecnik, J. Mora, N. Jabado, M. D. Taylor, A. Huang, E. Aronica, A. Bertoni, B. Radlwimmer, T. Pietsch, U. Schuller, R. Schneppenheim, P. A. Northcott, J. O. Korbel, R. Siebert, M. C. Fruhwald, P. Lichter, R. Eils, A. Gajjar, M. Hasselblatt, S. M. Pfister, M. Kool, Atypical Teratoid/Rhabdoid Tumors Are Comprised of Three Epigenetic Subgroups with Distinct Enhancer Landscapes. Cancer Cell 29, 379-393 (2016).

15. H. E. Chun, P. D. Johann, K. Milne, M. Zapatka, A. Buellesbach, N. Ishaque, M. Iskar, S. Erkek, L. Wei, B. Tessier-Cloutier, J. Lever, E. Titmuss, J. T. Topham, R. Bowlby, E. Chuah, K. L. Mungall, Y. Ma, A. J. Mungall, R. A. Moore, M. D. Taylor, D. S. Gerhard, S. J. M. Jones, A. Korshunov, M. Gessler, K. Kerl, M. Hasselblatt, M. C. Fruhwald, E. J. Perlman, B. H. Nelson, S. M. Pfister, M. A. Marra, M. Kool, Identification and Analyses of Extra-Cranial and Cranial Rhabdoid Tumor Molecular Subgroups Reveal Tumors with Cytotoxic T Cell Infiltration. Cell reports 29, 2338-2354.e2337 (2019).

16. S. Jessa, A. Blanchet-Cohen, B. Krug, M. Vladoiu, M. Coutelier, D. Faury, B. Poreau, N. De Jay, S. Hébert, J. Monlong, W. T. Farmer, L. K. Donovan, Y. Hu, M. K. McConechy, F. M. G. Cavalli, L. G. Mikael, B. Ellezam, M. Richer, A. Allaire, A. G. Weil, J. Atkinson, J.-P. Farmer, R. W. R. Dudley, V. Larouche, L. Crevier, S. Albrecht, M. G. Filbin, H. Sartelet, P.-E. Lutz, C. Nagy, G. Turecki, S. Costantino, P. B. Dirks, K. K. Murai, G. Bourque, J. Ragoussis, L. Garzia, M. D. Taylor, N. Jabado, C. L. Kleinman, Stalled developmental programs at the root of pediatric brain tumors. Nature Genetics 51, 1702-1713 (2019).

17. B. R. Cairns, Chromatin remodeling: insights and intrigue from single-molecule studies. Nature structural molecular biology 14, 989-996 (2007).

18. N. Kaplan, I. K. Moore, Y. Fondufe-Mittendorf, A. J. Gossett, D. Tillo, Y. Field, E. M. LeProust, T. R. Hughes, J. D. Lieb, J. Widom, E. Segal, The DNA-encoded nucleosome organization of a eukaryotic genome. Nature 458, 362-366 (2009).

19. C. Jiang, B. F. Pugh, Nucleosome positioning and gene regulation: advances through genomics. Nature reviews. Genetics 10, 161-172 (2009).

20. I. Whitehouse, O. J. Rando, J. Delrow, T. Tsukiyama, Chromatin remodelling at promoters suppresses antisense transcription. Nature 450, 1031-1035 (2007).

21. A. H. Shain, J. R. Pollack, The spectrum of SWI/SNF mutations, ubiquitous in human cancers. PloS one 8, e55119 (2013).

22. C. Kadoch, R. T. Williams, J. P. Calarco, E. L. Miller, C. M. Weber, S. M. Braun, J. L. Pulice, E. J. Chory, G. R. Crabtree, Dynamics of BAF-Polycomb complex opposition on heterochromatin in normal and oncogenic states. Nat Genet 49, 213-222 (2017).

23. M. Y. Tolstorukov, C. G. Sansam, P. Lu, E. C. Koellhoffer, K. C. Helming, B. H. Alver, E. J. Tillman, J. A. Evans, B. G. Wilson, P. J. Park, C. W. M. Roberts, Swi/Snf chromatin

remodeling/tumor suppressor complex establishes nucleosome occupancy at target promoters. Proceedings of the National Academy of Sciences of the United States of America 110, 10165-10170 (2013).

24. X. Wang, R. S. Lee, B. H. Alver, J. R. Haswell, S. Wang, J. Mieczkowski, Y. Drier, S. M. Gillespie, T. C. Archer, J. N. Wu, E. P. Tzvetkov, E. C. Troisi, S. L. Pomeroy, J. A. Biegel, M. Y. Tolstorukov, B. E. Bernstein, P. J. Park, C. W. M. Roberts, SMARCB1-mediated SWI/SNF complex function is essential for enhancer regulation. Nat Genet 49, 289-295 (2017).

25. R. T. Nakayama, J. L. Pulice, A. M. Valencia, M. J. McBride, Z. M. McKenzie, M. A. Gillespie, W. L. Ku, M. Teng, K. Cui, R. T. Williams, S. H. Cassel, H. Qing, C. J. Widmer, G. D. Demetri, R. A. Irizarry, K. Zhao, J. A. Ranish, C. Kadoch, SMARCB1 is required for widespread BAF complex-mediated activation of enhancers and bivalent promoters. Nature Genetics, (2017).

26. Y. Han, A. A. Reyes, S. Malik, Y. He, Cryo-EM structure of SWI/SNF complex bound to a nucleosome. Nature 579, 452-455 (2020).

27. D. N. Doan, T. M. Veal, Z. Yan, W. Wang, S. N. Jones, A. N. Imbalzano, Loss of the INI1 tumor suppressor does not impair the expression of multiple BRG1-dependent genes or the assembly of SWI/SNF enzymes. Oncogene 23, 3462-3473 (2004).

28. D. Wei, D. Goldfarb, S. Song, C. Cannon, F. Yan, D. Sakellariou-Thompson, SNF5/INI1 deficiency redefines chromatin remodeling complex composition during tumor development. Mol Cancer Res 12, (2014).

29. X. Wang, C. G. Sansam, C. S. Thom, D. Metzger, J. A. Evans, P. T. L. Nguyen, C. W. M. Roberts, Oncogenesis caused by loss of the SNF5 tumor suppressor is dependent on activity of BRG1, the ATPase of the SWI/SNF chromatin remodeling complex. Cancer research 69, 8094-8101 (2009).

30. J. A. West, A. Cook, B. H. Alver, M. Stadtfeld, A. M. Deaton, K. Hochedlinger, P. J. Park, M. Y. Tolstorukov, R. E. Kingston, Nucleosomal occupancy changes locally over key regulatory regions during cell differentiation and reprogramming. Nature Communications 5, 4719 (2014).

31. J. S. You, D. D. De Carvalho, C. Dai, M. Liu, K. Pandiyan, X. J. Zhou, G. Liang, P. A. Jones, SNF5 is an essential executor of epigenetic regulation during differentiation. PLoS genetics 9, e1003459 (2013).

32. L. Ho, J. L. Ronan, J. Wu, B. T. Staahl, L. Chen, A. Kuo, J. Lessard, A. I. Nesvizhskii, J. Ranish, G. R. Crabtree, An embryonic stem cell chromatin remodeling complex, esBAF, is essential for embryonic stem cell self-renewal and pluripotency. Proceedings of the National Academy of Sciences of the United States of America 106, 5181-5186 (2009).

33. B. T. Staahl, J. Tang, W. Wu, A. Sun, A. D. Gitler, A. S. Yoo, G. R. Crabtree, Kinetic Analysis of npBAF to nBAF Switching Reveals Exchange of SS18 with CREST and Integration with Neural Developmental Pathways. The Journal of Neuroscience 33, 10348-10361 (2013).

34. J. Lessard, J. I. Wu, J. A. Ranish, M. Wan, M. M. Winslow, B. T. Staahl, H. Wu, R. Aebersold, I. A. Graef, G. R. Crabtree, An essential switch in subunit composition of a chromatin remodeling complex during neural development. Neuron 55, 201-215 (2007).

35. L. Ho, G. R. Crabtree, Chromatin remodelling during development. Nature 463, 474-484 (2010).

36. O. A. Romero, M. Sanchez-Cespedes, The SWI/SNF genetic blockade: effects in cell differentiation, cancer and developmental diseases. Oncogene 33, 2681-2689 (2013).

37. N. Singhal, J. Graumann, G. Wu, M. J. Araúzo-Bravo, D. W. Han, B. Greber, L. Gentile, M. Mann, H. R. Schöler, Chromatin-Remodeling Components of the BAF Complex Facilitate Reprogramming. Cell 141, 943-955 (2010).

38. B. G. Wilson, X. Wang, X. Shen, E. S. McKenna, M. E. Lemieux, Y.-J. Cho, E. C. Koellhoffer, S. L. Pomeroy, S. H. Orkin, C. W. M. Roberts, Epigenetic antagonism between polycomb and SWI/SNF complexes during oncogenic transformation. Cancer cell 18, 316-328 (2010).

39. R. Margueron, D. Reinberg, The Polycomb complex PRC2 and its mark in life. Nature 469, 343-349 (2011).

40. C. W. M. Roberts, S. A. Galusha, M. E. McMenamin, C. D. M. Fletcher, S. H. Orkin, Haploinsufficiency of Snf5 (integrase interactor 1) predisposes to malignant rhabdoid tumors in mice. (2000).

41. T. Koga, I. A. Chaim, J. A. Benitez, S. Markmiller, A. D. Parisian, R. F. Hevner, K. M. Turner, F. M. Hessenauer, M. D'Antonio, N.-p. D. Nguyen, S. Saberi, J. Ma, S. Miki, A. D. Boyer, J. Ravits, K. A. Frazer, V. Bafna, C. C. Chen, P. S. Mischel, G. W. Yeo, F. B. Furnari, Longitudinal assessment of tumor development using cancer avatars derived from genetically engineered pluripotent stem cells. Nature Communications 11, 550 (2020).

42. M. Jinek, K. Chylinski, I. Fonfara, M. Hauer, J. A. Doudna, E. Charpentier, A programmable dual-RNA-guided DNA endonuclease in adaptive bacterial immunity. Science (New York, N.Y.) 337, 816-821 (2012).

43. A. Veres, B. S. Gosis, Q. Ding, R. Collins, A. Ragavendran, H. Brand, S. Erdin, C. A. Cowan, M. E. Talkowski, K. Musunuru, Low incidence of off-target mutations in individual CRISPR-Cas9 and TALEN targeted human stem cell clones detected by whole-genome sequencing. Cell stem cell 15, 27-30 (2014).

44. L. Cong, F. A. Ran, D. Cox, S. Lin, R. Barretto, N. Habib, P. D. Hsu, X. Wu, W. Jiang, L. A. Marraffini, F. Zhang, Multiplex genome engineering using CRISPR/Cas systems. Science (New York, N.Y.) 339, 819-823 (2013).

45. Mohammad A. Mandegar, N. Huebsch, Ekaterina B. Frolov, E. Shin, A. Truong, Michael P. Olvera, Amanda H. Chan, Y. Miyaoka, K. Holmes, C. I. Spencer, Luke M. Judge, David E. Gordon, Tilde V. Eskildsen, Jacqueline E. Villalta, Max A. Horlbeck, Luke A. Gilbert, Nevan J. Krogan, Søren P. Sheikh, Jonathan S. Weissman, Lei S. Qi, P.-L. So, Bruce R. Conklin, CRISPR Interference Efficiently Induces Specific and Reversible Gene Silencing in Human iPSCs. Cell Stem Cell 18, 541-553 (2016).

46. K. Labun, T. G. Montague, M. Krause, Y. N. Torres Cleuren, H. Tjeldnes, E. Valen, CHOPCHOP v3: expanding the CRISPR web toolbox beyond genome editing. Nucleic Acids Research 47, W171-W174 (2019).

47. A. S. Yoo, B. T. Staahl, L. Chen, G. R. Crabtree, MicroRNA-mediated switching of chromatin-remodelling complexes in neural development. Nature 460, 642-646 (2009).

48. J. R. Dixon, I. Jung, S. Selvaraj, Y. Shen, J. E. Antosiewicz-Bourget, A. Y. Lee, Z. Ye, A. Kim, N. Rajagopal, W. Xie, Y. Diao, J. Liang, H. Zhao, V. V. Lobanenkov, J. R. Ecker, J. A. Thomson, B. Ren, Chromatin architecture reorganization during stem cell differentiation. Nature 518, 331-336 (2015).

49. P. Reinhardt, M. Glatza, K. Hemmer, Y. Tsytsyura, C. S. Thiel, S. Hoing, S. Moritz, J. A. Parga, L. Wagner, J. M. Bruder, G. Wu, B. Schmid, A. Ropke, J. Klingauf, J. C. Schwamborn, T. Gasser, H. R. Scholer, J. Sterneckert, Derivation and expansion using only small molecules of human neural progenitors for neurodegenerative disease modeling. PLoS One 8, e59252 (2013).

50. S. Erkek, P. D. Johann, M. A. Finetti, Y. Drosos, H.-C. Chou, M. Zapatka, D. Sturm, D. T. W. Jones, A. Korshunov, M. Rhyzova, S. Wolf, J.-P. Mallm, K. Beck, O. Witt, A. E. Kulozik, M. C. Frühwald, P. A. Northcott, J. O. Korbel, P. Lichter, R. Eils, A. Gajjar, C. W. M. Roberts, D. Williamson, M. Hasselblatt, L. Chavez, S. M. Pfister, M. Kool, Comprehensive Analysis of Chromatin States in Atypical Teratoid/Rhabdoid Tumor Identifies Diverging Roles for SWI/SNF and Polycomb in Gene Regulation. Cancer Cell 35, 95-110.e118 (2019).

51. M. A. Lancaster, J. A. Knoblich, Generation of cerebral organoids from human pluripotent stem cells. Nature protocols 9, 2329-2340 (2014).

52. M. A. Lancaster, M. Renner, C.-A. Martin, D. Wenzel, L. S. Bicknell, M. E. Hurles, T. Homfray, J. M. Penninger, A. P. Jackson, J. A. Knoblich, Cerebral organoids model human brain development and microcephaly. Nature 501, 373-379 (2013).

53. A. Butler, P. Hoffman, P. Smibert, E. Papalexi, R. Satija, Integrating single-cell transcriptomic data across different conditions, technologies, and species. Nature Biotechnology 36, 411-420 (2018).

54. K. Street, D. Risso, R. B. Fletcher, D. Das, J. Ngai, N. Yosef, E. Purdom, S. Dudoit, Slingshot: cell lineage and pseudotime inference for single-cell transcriptomics. BMC Genomics 19, 477-477 (2018).

55. E. Eden, R. Navon, I. Steinfeld, D. Lipson, Z. Yakhini, GOrilla: a tool for discovery and visualization of enriched GO terms in ranked gene lists. BMC Bioinformatics 10, 48 (2009).

56. I. Versteege, N. Sévenet, J. Lange, M. F. Rousseau-Merck, P. Ambros, R. Handgretinger, A. Aurias, O. Delattre, Truncating mutations of hSNF5/INI1 in aggressive paediatric cancer. Nature 394, 203-206 (1998).

57. P. Johann, A. Korshunov, K. Kerl, A. Huang, N. Jabado, M. Hasselblatt, M. Frühwald, S. Pfister, M. Kool, CNS AT/RTs are a Heterogeneous Entity That Comprises Subgroups with Distinct Molecular Profiles. Cancer Genetics 207, 447 (2014).

58. L. F. Langer, J. M. Ward, T. K. Archer, Tumor suppressor SMARCB1 suppresses super-enhancers to govern hESC lineage determination. eLife 8, (2019).

59. H.-Jung E. Chun, Emilia L. Lim, A. Heravi-Moussavi, S. Saberi, Karen L. Mungall, M. Bilenky, A. Carles, K. Tse, I. Shlafman, K. Zhu, Jenny Q. Qian, Diana L. Palmquist, A. He, W. Long, R. Goya, M. Ng, Veronique G. LeBlanc, E. Pleasance, N. Thiessen, T. Wong, E. Chuah, Y.-J. Zhao, Jacquie E. Schein, Daniela S. Gerhard, Michael D. Taylor, Andrew J. Mungall, Richard A. Moore, Y. Ma, Steven J. M. Jones, Elizabeth J. Perlman, M. Hirst, Marco A. Marra, Genome-Wide Profiles of Extra-cranial Malignant Rhabdoid Tumors Reveal Heterogeneity and Dysregulated Developmental Pathways. Cancer Cell 29, 394-406 (2016).

60. M. I. Love, W. Huber, S. Anders, Moderated estimation of fold change and dispersion for RNA-seq data with DESeq2. Genome Biology 15, 550 (2014).

61. U. Raudvere, L. Kolberg, I. Kuzmin, T. Arak, P. Adler, H. Peterson, J. Vilo, g:Profiler: a web server for functional enrichment analysis and conversions of gene lists (2019 update). Nucleic Acids Research 47, W191-W198 (2019).

62. P. Shannon, A. Markiel, O. Ozier, N. S. Baliga, J. T. Wang, D. Ramage, N. Amin, B. Schwikowski, T. Ideker, Cytoscape: a software environment for integrated models of biomolecular interaction networks. Genome Res 13, 2498-2504 (2003).

63. D. Merico, R. Isserlin, O. Stueker, A. Emili, G. D. Bader, Enrichment map: a network-based method for gene-set enrichment visualization and interpretation. PLoS One 5, e13984 (2010).